Tests of general relativity with GW150914

B. P. Abbott[1], R. Abbott[1], T. D. Abbott[2], M. R. Abernathy[1], F. Acernese[3,4], K. Ackley[5], C. Adams[6], T. Adams[7], P. Addesso[3], R. X. Adhikari[1], V. B. Adya[8], C. Affeldt[8], M. Agathos[9], K. Agatsuma[9], N. Aggarwal[10], O. D. Aguiar[11], L. Aiello[12,13], A. Ain[14], P. Ajith[15], B. Allen[8,16,17], A. Allocca[18,19], P. A. Altin[20], S. B. Anderson[1], W. G. Anderson[16], K. Arai[1], M. C. Araya[1], C. C. Arceneaux[21], J. S. Areeda[22], N. Arnaud[23], K. G. Arun[24], S. Ascenzi[25,13], G. Ashton[26], M. Ast[27], S. M. Aston[6], P. Astone[28], P. Aufmuth[8], C. Aulbert[8], S. Babak[29], P. Bacon[30], M. K. M. Bader[9], P. T. Baker[31], F. Baldaccini[32,33], G. Ballardin[34], S. W. Ballmer[35], J. C. Barayoga[1], S. E. Barclay[36], B. C. Barish[1], D. Barker[37], F. Barone[3,4], B. Barr[36], L. Barsotti[10], M. Barsuglia[30], D. Barta[38], J. Bartlett[37], I. Bartos[39], R. Bassiri[40], A. Basti[18,19], J. C. Batch[37], C. Baune[8], V. Bavigadda[34], M. Bazzan[41,42], B. Behnke[29], M. Bejger[43], C. Belczynski[44], A. S. Bell[36], C. J. Bell[36], B. K. Berger[1], J. Bergman[37], G. Bergmann[8], C. P. L. Berry[45], D. Bersanetti[46,47], A. Bertolini[9], J. Betzwieser[6], S. Bhagwat[35], R. Bhandare[48], I. A. Bilenko[49], G. Billingsley[1], J. Birch[6], R. Birney[50], O. Birnholtz[8], S. Biscans[10], A. Bisht[8,17], M. Bitossi[34], C. Biwer[35], M. A. Bizouard[23], J. K. Blackburn[1], C. D. Blair[51], D. G. Blair[51], R. M. Blair[37], S. Bloemen[52], O. Bock[8], T. P. Bodiya[10], M. Boer[53], G. Bogaert[53], C. Bogan[8], A. Bohe[29], P. Bojtos[54], C. Bond[45], F. Bondu[55], R. Bonnand[7], B. A. Boom[9], R. Bork[1], V. Boschi[18,19], S. Bose[56,14], Y. Bouffanais[30], M. Boyle[134], A. Bozzi[34], C. Bradaschia[19], P. R. Brady[16], V. B. Braginsky[49], M. Branchesi[57,58], J. E. Brau[59], T. Briant[60], A. Brillet[53], M. Brinkmann[8], V. Brisson[23], P. Brockill[16], A. F. Brooks[1], D. A. Brown[35], D. D. Brown[45], N. M. Brown[10], C. C. Buchanan[2], A. Buikema[10], T. Bulik[44], H. J. Bulten[61,9], A. Buonanno[29,62], D. Buskulic[7], C. Buy[30], R. L. Byer[40], L. Cadonati[63], G. Cagnoli[64,65], C. Cahillane[1], J. Calderón Bustillo[66,63], T. Callister[1], E. Calloni[67,4], J. B. Camp[68], K. C. Cannon[69], J. Cao[70], C. D. Capano[8], E. Capocasa[30], F. Carbognani[34], S. Caride[71], J. Casanueva Diaz[23], C. Casentini[25,13], S. Caudill[16], M. Cavaglià[21], F. Cavalier[23], R. Cavalieri[34], G. Cella[19], C. Cepeda[1], L. Cerboni Baiardi[57,58], G. Cerretani[18,19], E. Cesarini[25,13], R. Chakraborty[1], T. Chalermsongsak[1], S. J. Chamberlin[72], M. Chan[36], S. Chao[73], P. Charlton[74], E. Chassande-Mottin[30], H. Y. Chen[75], Y. Chen[76], C. Cheng[73], A. Chincarini[47], A. Chiummo[34], H. S. Cho[77], M. Cho[62], J. H. Chow[20], N. Christensen[78], Q. Chu[51], S. Chua[60], S. Chung[51], G. Ciani[5], F. Clara[37], J. A. Clark[63], F. Cleva[53], E. Coccia[25,12,13], P.-F. Cohadon[60], A. Colla[79,28], C. G. Collette[80], L. Cominsky[81], M. Constancio Jr.[11], A. Conte[79,28], L. Conti[42], D. Cook[37], T. R. Corbitt[2], N. Cornish[31], A. Corsi[82], S. Cortese[34], C. A. Costa[11], M. W. Coughlin[78], S. B. Coughlin[83], J.-P. Coulon[53], S. T. Countryman[39], P. Couvares[1], E. E. Cowan[63], D. M. Coward[51], M. J. Cowart[6], D. C. Coyne[1], R. Coyne[82], K. Craig[36], J. D. E. Creighton[16], J. Cripe[2], S. G. Crowder[84], A. Cumming[36], L. Cunningham[36], E. Cuoco[34], T. Dal Canton[8], S. L. Danilishin[36], S. D'Antonio[13], K. Danzmann[17,8], N. S. Darman[85], V. Dattilo[34], I. Dave[48], H. P. Daveloza[86], M. Davier[23], G. S. Davies[36], E. J. Daw[87], R. Day[34], D. DeBra[40], G. Debreczeni[38], J. Degallaix[65], M. De Laurentis[67,4], S. Deléglise[60], W. Del Pozzo[45], T. Denker[8,17], T. Dent[8], H. Dereli[53], V. Dergachev[1], R. T. DeRosa[6], R. De Rosa[67,4], R. DeSalvo[88], S. Dhurandhar[14], M. C. Díaz[86], L. Di Fiore[4], M. Di Giovanni[79,28], A. Di Lieto[18,19], S. Di Pace[79,28], I. Di Palma[29,8], A. Di Virgilio[19], G. Dojcinoski[89], V. Dolique[65], F. Donovan[10], K. L. Dooley[21], S. Doravari[6,8], R. Douglas[36], T. P. Downes[16], M. Drago[8,90,91], R. W. P. Drever[1], J. C. Driggers[37], Z. Du[70], M. Ducrot[7], S. E. Dwyer[37], T. B. Edo[87], M. C. Edwards[78], A. Effler[6], H.-B. Eggenstein[8], P. Ehrens[1], J. Eichholz[5], S. S. Eikenberry[5], W. Engels[76], R. C. Essick[10], T. Etzel[1], M. Evans[10], T. M. Evans[6], R. Everett[72], M. Factourovich[39], V. Fafone[25,13,12], H. Fair[35], S. Fairhurst[92], X. Fan[70], Q. Fang[51], S. Farinon[47], B. Farr[75], W. M. Farr[45], M. Favata[89], M. Fays[92], H. Fehrmann[8], M. M. Fejer[40], I. Ferrante[18,19], E. C. Ferreira[11], F. Ferrini[34], F. Fidecaro[18,19], I. Fiori[34], D. Fiorucci[30], R. P. Fisher[35], R. Flaminio[65,93], M. Fletcher[36], J.-D. Fournier[53], S. Franco[23], S. Frasca[79,28], F. Frasconi[19], Z. Frei[54], A. Freise[45], R. Frey[59], V. Frey[23], T. T. Fricke[8], P. Fritschel[10], V. V. Frolov[6], P. Fulda[5], M. Fyffe[6], H. A. G. Gabbard[21], J. R. Gair[94], L. Gammaitoni[32,33], S. G. Gaonkar[14], F. Garufi[67,4], A. Gatto[30], G. Gaur[95,96], N. Gehrels[68], G. Gemme[47], B. Gendre[53], E. Genin[34], A. Gennai[19], J. George[48], L. Gergely[97], V. Germain[7], Abhirup Ghosh[15], Archisman Ghosh[15], S. Ghosh[52,9], J. A. Giaime[2,6], K. D. Giardina[6], A. Giazotto[19], K. Gill[98], A. Glaefke[36], E. Goetz[71], R. Goetz[5], L. Gondan[54], G. González[2], J. M. Gonzalez Castro[18,19], A. Gopakumar[99], N. A. Gordon[36], M. L. Gorodetsky[49], S. E. Gossan[1], M. Gosselin[34], R. Gouaty[7], C. Graef[36], P. B. Graff[62], M. Granata[65], A. Grant[36], S. Gras[10], C. Gray[37], G. Greco[57,58], A. C. Green[45], P. Groot[52], H. Grote[8], S. Grunewald[29], G. M. Guidi[57,58], X. Guo[70], A. Gupta[14], M. K. Gupta[96], K. E. Gushwa[1], E. K. Gustafson[1], R. Gustafson[71], J. J. Hacker[22], B. R. Hall[56], E. D. Hall[1], G. Hammond[36], M. Haney[99], M. M. Hanke[8], J. Hanks[37], C. Hanna[72], M. D. Hannam[92], J. Hanson[6], T. Hardwick[2], J. Harms[57,58], G. M. Harry[100], I. W. Harry[29], M. J. Hart[36], M. T. Hartman[5], C.-J. Haster[45], K. Haughian[36], J. Healy[112], A. Heidmann[60], M. C. Heintze[5,6], H. Heitmann[53], P. Hello[23], D. Hemberger[76], G. Hemming[34], M. Hendry[36], I. S. Heng[36], J. Hennig[36], A. W. Heptonstall[1], M. Heurs[8,17], S. Hild[36], D. Hoak[101], K. A. Hodge[1], D. Hofman[65], S. E. Hollitt[102], K. Holt[6], D. E. Holz[75], P. Hopkins[92], D. J. Hosken[102], J. Hough[36], E. A. Houston[36], E. J. Howell[51], Y. M. Hu[36], S. Huang[73], E. A. Huerta[103,83], D. Huet[23], B. Hughey[98], S. Husa[66], S. H. Huttner[36], T. Huynh-Dinh[6], A. Idrisy[72], N. Indik[8], D. R. Ingram[37], R. Inta[82], H. N. Isa[36], J.-M. Isac[60], M. Isi[1], G. Islas[22], T. Isogai[10], B. R. Iyer[15], K. Izumi[37], T. Jacqmin[60], H. Jang[77], K. Jani[63],

P. Jaranowski[104], S. Jawahar[105], F. Jiménez-Forteza[66], W. W. Johnson[2], D. I. Jones[26], R. Jones[36], R. J. G. Jonker[9], L. Ju[51], Haris K[106], C. V. Kalaghatgi[24,92], V. Kalogera[83], S. Kandhasamy[21], G. Kang[77], J. B. Kanner[1], S. Karki[59], M. Kasprzack[2,23,34], E. Katsavounidis[10], W. Katzman[6], S. Kaufer[17], T. Kaur[51], K. Kawabe[37], F. Kawazoe[8], F. Kéfélian[53], M. S. Kehl[69], D. Keitel[8,66], D. B. Kelley[35], W. Kells[1], R. Kennedy[87], J. S. Key[86], A. Khalaidovski[8], F. Y. Khalili[49], I. Khan[12], S. Khan[92], Z. Khan[96], E. A. Khazanov[107], L. E. Kidder[134], N. Kijbunchoo[37], C. Kim[77], J. Kim[108], K. Kim[109], Nam-Gyu Kim[77], Namjun Kim[40], Y.-M. Kim[108], E. J. King[102], P. J. King[37], D. L. Kinzel[6], J. S. Kissel[37], L. Kleybolte[27], S. Klimenko[5], S. M. Koehlenbeck[8], K. Kokeyama[2], S. Koley[9], V. Kondrashov[1], A. Kontos[10], M. Korobko[27], W. Z. Korth[1], I. Kowalska[44], D. B. Kozak[1], V. Kringel[8], B. Krishnan[8], A. Królak[110,111], C. Krueger[17], G. Kuehn[8], P. Kumar[69], L. Kuo[73], A. Kutynia[110], B. D. Lackey[35], M. Landry[37], J. Lange[112], B. Lantz[40], P. D. Lasky[113], A. Lazzarini[1], C. Lazzaro[63,42], P. Leaci[29,79,28], S. Leavey[36], E. O. Lebigot[30,70], C. H. Lee[108], H. K. Lee[109], H. M. Lee[114], K. Lee[36], A. Lenon[35], M. Leonardi[90,91], J. R. Leong[8], N. Leroy[23], N. Letendre[7], Y. Levin[113], B. M. Levine[37], T. G. F. Li[1], A. Libson[10], T. B. Littenberg[115], N. A. Lockerbie[105], J. Logue[36], A. L. Lombardi[101], L. London[91], J. E. Lord[35], M. Lorenzini[12,13], V. Loriette[116], M. Lormand[6], G. Losurdo[58], J. D. Lough[8,17], C. O. Lousto[112], G. Lovelace[22], H. Lück[17,8], A. P. Lundgren[8], J. Luo[78], R. Lynch[10], Y. Ma[51], T. MacDonald[40], B. Machenschalk[8], M. MacInnis[10], D. M. Macleod[2], F. Magaña-Sandoval[35], R. M. Magee[56], M. Mageswaran[1], E. Majorana[28], I. Maksimovic[116], V. Malvezzi[25,13], N. Man[53], I. Mandel[45], V. Mandic[84], V. Mangano[36], G. L. Mansell[20], M. Manske[16], M. Mantovani[34], F. Marchesoni[117,33], F. Marion[7], S. Márka[39], Z. Márka[39], A. S. Markosyan[40], E. Maros[1], F. Martelli[57,58], L. Martellini[53], I. W. Martin[36], R. M. Martin[5], D. V. Martynov[1], J. N. Marx[1], K. Mason[10], A. Masserot[7], T. J. Massinger[35], M. Masso-Reid[36], F. Matichard[10], L. Matone[39], N. Mavalvala[10], N. Mazumder[56], G. Mazzolo[8], R. McCarthy[37], D. E. McClelland[20], S. McCormick[6], S. C. McGuire[118], G. McIntyre[1], J. McIver[101], D. J. McManus[20], S. T. McWilliams[103], D. Meacher[72], G. D. Meadors[29,8], J. Meidam[9], A. Melatos[85], G. Mendell[37], D. Mendoza-Gandara[8], R. A. Mercer[16], E. Merilh[37], M. Merzougui[53], S. Meshkov[1], C. Messenger[36], C. Messick[72], P. M. Meyers[84], F. Mezzani[28,79], H. Miao[45], C. Michel[65], H. Middleton[45], E. E. Mikhailov[119], K. N. Mukund[14], L. Milano[67,4], J. Miller[10], M. Millhouse[31], Y. Minenkov[13], J. Ming[29,8], S. Mirshekari[120], C. Mishra[15], S. Mitra[14], V. P. Mitrofanov[49], G. Mitselmakher[5], R. Mittleman[10], A. Moggi[19], M. Mohan[34], S. R. P. Mohapatra[10], M. Montani[57,58], B. C. Moore[89], C. J. Moore[121], D. Moraru[37], G. Moreno[37], S. R. Morriss[86], K. Mossavi[8], B. Mours[7], C. M. Mow-Lowry[45], C. L. Mueller[5], G. Mueller[5], A. W. Muir[92], Arunava Mukherjee[15], D. Mukherjee[16], S. Mukherjee[86], A. Mullavey[6], J. Munch[102], D. J. Murphy[39], P. G. Murray[36], A. Mytidis[5], I. Nardecchia[25,13], L. Naticchioni[79,28], R. K. Nayak[122], V. Necula[5], K. Nedkova[101], G. Nelemans[52,9], M. Neri[46,47], A. Neunzert[71], G. Newton[36], T. T. Nguyen[20], A. B. Nielsen[8], S. Nissanke[52,9], A. Nitz[8], F. Nocera[34], D. Nolting[6], M. E. N. Normandin[86], L. K. Nuttall[35], J. Oberling[37], E. Ochsner[16], J. O'Dell[123], E. Oelker[10], G. H. Ogin[124], J. J. Oh[125], S. H. Oh[125], F. Ohme[92], M. Oliver[66], P. Oppermann[8], Richard J. Oram[6], B. O'Reilly[6], R. O'Shaughnessy[112], S. Ossokine[29], C. D. Ott[76], D. J. Ottaway[102], R. S. Ottens[5], H. Overmier[6], B. J. Owen[82], A. Pai[106], S. A. Pai[48], J. R. Palamos[59], O. Palashov[107], C. Palomba[28], A. Pal-Singh[27], H. Pan[73], C. Pankow[83], F. Pannarale[92], B. C. Pant[48], F. Paoletti[34,19], A. Paoli[34], Y. Pan[62], M. A. Papa[29,16,8], H. R. Paris[40], W. Parker[6], D. Pascucci[36], A. Pasqualetti[34], R. Passaquieti[18,19], D. Passuello[19], B. Patricelli[18,19], Z. Patrick[40], B. L. Pearlstone[36], M. Pedraza[1], R. Pedurand[65], L. Pekowsky[35], A. Pele[6], S. Penn[126], A. Perreca[1], M. Phelps[36], O. Piccinni[79,28], M. Pichot[53], F. Piergiovanni[57,58], V. Pierro[88], G. Pillant[34], L. Pinard[65], I. M. Pinto[88], M. Pitkin[36], H. P. Pfeiffer[69], R. Poggiani[18,19], P. Popolizio[34], A. Post[8], J. Powell[36], J. Prasad[14], V. Predoi[92], S. S. Premachandra[113], T. Prestegard[84], L. R. Price[1], M. Prijatelj[34], M. Principe[88], S. Privitera[29], R. Prix[8], G. A. Prodi[90,91], L. Prokhorov[49], O. Puncken[8], M. Punturo[33], P. Puppo[28], M. Pürrer[29], H. Qi[16], J. Qin[51], V. Quetschke[86], E. A. Quintero[1], R. Quitzow-James[59], F. J. Raab[37], D. S. Rabeling[20], H. Radkins[37], P. Raffai[54], S. Raja[48], M. Rakhmanov[86], P. Rapagnani[79,28], V. Raymond[29], M. Razzano[18,19], V. Re[25], J. Read[22], C. M. Reed[37], T. Regimbau[53], L. Rei[47], S. Reid[50], D. H. Reitze[1,5], H. Rew[119], S. D. Reyes[35], F. Ricci[79,28], K. Riles[71], N. A. Robertson[1,36], R. Robie[36], F. Robinet[23], A. Rocchi[13], L. Rolland[7], J. G. Rollins[1], V. J. Roma[59], R. Romano[3,4], G. Romanov[119], J. H. Romie[6], D. Rosińska[127,43], S. Rowan[36], A. Rüdiger[8], P. Ruggi[34], K. Ryan[37], S. Sachdev[1], T. Sadecki[37], L. Sadeghian[16], L. Salconi[34], M. Saleem[106], F. Salemi[8], A. Samajdar[122], L. Sammut[85,113], E. J. Sanchez[1], V. Sandberg[37], B. Sandeen[83], J. R. Sanders[71,35], B. Sassolas[65], B. S. Sathyaprakash[92], P. R. Saulson[35], O. Sauter[71], R. L. Savage[37], A. Sawadsky[17], P. Schale[59], M. Scheel[76], R. Schilling[†8], J. Schmidt[8], P. Schmidt[1,76], R. Schnabel[27], R. M. S. Schofield[59], A. Schönbeck[27], E. Schreiber[8], D. Schuette[8,17], B. F. Schutz[92], J. Scott[36], S. M. Scott[20], D. Sellers[6], D. Sentenac[34], V. Sequino[25,13], A. Sergeev[107], G. Serna[22], Y. Setyawati[52,9], A. Sevigny[37], D. A. Shaddock[20], S. Shah[52,9], M. S. Shahriar[83], M. Shaltev[8], Z. Shao[1], B. Shapiro[40], P. Shawhan[62], A. Sheperd[16], D. H. Shoemaker[10], D. M. Shoemaker[63], K. Siellez[53,63], X. Siemens[16], D. Sigg[37], A. D. Silva[11], D. Simakov[8], A. Singer[1], L. P. Singer[68], A. Singh[29,8], R. Singh[2], A. Singhal[12], A. M. Sintes[66], B. J. J. Slagmolen[20], J. R. Smith[22], N. D. Smith[1], R. J. E. Smith[1], E. J. Son[125], B. Sorazu[36], F. Sorrentino[47], T. Souradeep[14], A. K. Srivastava[96], A. Staley[39], M. Steinke[8], J. Steinlechner[36], S. Steinlechner[36], D. Steinmeyer[8,17], B. C. Stephens[16], R. Stone[86], K. A. Strain[36], N. Straniero[65],

G. Stratta[57,58], N. A. Strauss[78], S. Strigin[49], R. Sturani[120], A. L. Stuver[6], T. Z. Summerscales[128], L. Sun[85], P. J. Sutton[92], B. L. Swinkels[34], M. J. Szczepańczyk[98], B. Szilagyi[76], M. Tacca[30], D. Talukder[59], D. B. Tanner[5], M. Tápai[97], S. P. Tarabrin[8], A. Taracchini[29], R. Taylor[1], S. Teukolsky[134], T. Theeg[8], M. P. Thirugnanasambandam[1], E. G. Thomas[45], M. Thomas[6], P. Thomas[37], K. A. Thorne[6], K. S. Thorne[76], E. Thrane[113], S. Tiwari[12], V. Tiwari[92], K. V. Tokmakov[105], C. Tomlinson[87], M. Tonelli[18,19], C. V. Torres[‡86], C. I. Torrie[1], D. Töyrä[45], F. Travasso[32,33], G. Traylor[6], D. Trifirò[21], M. C. Tringali[90,91], L. Trozzo[129,19], M. Tse[10], M. Turconi[53], D. Tuyenbayev[86], D. Ugolini[130], C. S. Unnikrishnan[99], A. L. Urban[16], S. A. Usman[35], H. Vahlbruch[17], G. Vajente[1], G. Valdes[86], N. K. Johnson-McDaniel[15], M. Vallisneri[76], N. van Bakel[9], M. van Beuzekom[9], J. F. J. van den Brand[61,9], C. Van Den Broeck[9], D. C. Vander-Hyde[35,22], L. van der Schaaf[9], J. V. van Heijningen[9], A. A. van Veggel[36], M. Vardaro[41,42], S. Vass[1], M. Vasúth[38], R. Vaulin[10], A. Vecchio[45], G. Vedovato[42], J. Veitch[45], P. J. Veitch[102], K. Venkateswara[131], D. Verkindt[7], F. Vetrano[57,58], A. Viceré[57,58], S. Vinciguerra[45], D. J. Vine[50], J.-Y. Vinet[53], S. Vitale[10], T. Vo[35], H. Vocca[32,33], C. Vorvick[37], D. Voss[5], W. D. Vousden[45], S. P. Vyatchanin[49], A. R. Wade[20], L. E. Wade[132], M. Wade[132], M. Walker[2], L. Wallace[1], S. Walsh[16,8,29], G. Wang[12], H. Wang[45], M. Wang[45], X. Wang[70], Y. Wang[51], R. L. Ward[20], J. Warner[37], M. Was[7], B. Weaver[37], L.-W. Wei[53], M. Weinert[8], A. J. Weinstein[1], R. Weiss[10], T. Welborn[6], L. Wen[51], P. Weßels[8], T. Westphal[8], K. Wette[8], J. T. Whelan[112,8], D. J. White[87], B. F. Whiting[5], R. D. Williams[1], A. R. Williamson[92], J. L. Willis[133], B. Willke[17,8], M. H. Wimmer[8,17], W. Winkler[8], C. C. Wipf[1], H. Wittel[8,17], G. Woan[36], J. Worden[37], J. L. Wright[36], G. Wu[6], J. Yablon[83], W. Yam[10], H. Yamamoto[1], C. C. Yancey[62], M. J. Yap[20], H. Yu[10], M. Yvert[7], A. Zadrożny[110], L. Zangrando[42], M. Zanolin[98], J.-P. Zendri[42], M. Zevin[83], F. Zhang[10], L. Zhang[1], M. Zhang[119], Y. Zhang[112], C. Zhao[51], M. Zhou[83], Z. Zhou[83], X. J. Zhu[51], M. E. Zucker[1,10], S. E. Zuraw[101], and J. Zweizig[1]

(LIGO Scientific Collaboration and Virgo Collaboration)

[†]Deceased, May 2015. [‡]Deceased, March 2015.

[1]*LIGO, California Institute of Technology, Pasadena, CA 91125, USA*
[2]*Louisiana State University, Baton Rouge, LA 70803, USA*
[3]*Università di Salerno, Fisciano, I-84084 Salerno, Italy*
[4]*INFN, Sezione di Napoli, Complesso Universitario di Monte S.Angelo, I-80126 Napoli, Italy*
[5]*University of Florida, Gainesville, FL 32611, USA*
[6]*LIGO Livingston Observatory, Livingston, LA 70754, USA*
[7]*Laboratoire d'Annecy-le-Vieux de Physique des Particules (LAPP), Université Savoie Mont Blanc, CNRS/IN2P3, F-74941 Annecy-le-Vieux, France*
[8]*Albert-Einstein-Institut, Max-Planck-Institut für Gravitationsphysik, D-30167 Hannover, Germany*
[9]*Nikhef, Science Park, 1098 XG Amsterdam, The Netherlands*
[10]*LIGO, Massachusetts Institute of Technology, Cambridge, MA 02139, USA*
[11]*Instituto Nacional de Pesquisas Espaciais, 12227-010 São José dos Campos, SP, Brazil*
[12]*INFN, Gran Sasso Science Institute, I-67100 L'Aquila, Italy*
[13]*INFN, Sezione di Roma Tor Vergata, I-00133 Roma, Italy*
[14]*Inter-University Centre for Astronomy and Astrophysics, Pune 411007, India*
[15]*International Centre for Theoretical Sciences, Tata Institute of Fundamental Research, Bangalore 560012, India*
[16]*University of Wisconsin-Milwaukee, Milwaukee, WI 53201, USA*
[17]*Leibniz Universität Hannover, D-30167 Hannover, Germany*
[18]*Università di Pisa, I-56127 Pisa, Italy*
[19]*INFN, Sezione di Pisa, I-56127 Pisa, Italy*
[20]*Australian National University, Canberra, Australian Capital Territory 0200, Australia*
[21]*The University of Mississippi, University, MS 38677, USA*
[22]*California State University Fullerton, Fullerton, CA 92831, USA*
[23]*LAL, Univ. Paris-Sud, CNRS/IN2P3, Université Paris-Saclay, Orsay, France*
[24]*Chennai Mathematical Institute, Chennai, India*
[25]*Università di Roma Tor Vergata, I-00133 Roma, Italy*
[26]*University of Southampton, Southampton SO17 1BJ, United Kingdom*
[27]*Universität Hamburg, D-22761 Hamburg, Germany*
[28]*INFN, Sezione di Roma, I-00185 Roma, Italy*
[29]*Albert-Einstein-Institut, Max-Planck-Institut für Gravitationsphysik, D-14476 Potsdam-Golm, Germany*
[30]*APC, AstroParticule et Cosmologie, Université Paris Diderot, CNRS/IN2P3, CEA/Irfu, Observatoire de Paris, Sorbonne Paris Cité, F-75205 Paris Cedex 13, France*
[31]*Montana State University, Bozeman, MT 59717, USA*
[32]*Università di Perugia, I-06123 Perugia, Italy*
[33]*INFN, Sezione di Perugia, I-06123 Perugia, Italy*
[34]*European Gravitational Observatory (EGO), I-56021 Cascina, Pisa, Italy*
[35]*Syracuse University, Syracuse, NY 13244, USA*
[36]*SUPA, University of Glasgow, Glasgow G12 8QQ, United Kingdom*

[37]*LIGO Hanford Observatory, Richland, WA 99352, USA*
[38]*Wigner RCP, RMKI, H-1121 Budapest, Konkoly Thege Miklós út 29-33, Hungary*
[39]*Columbia University, New York, NY 10027, USA*
[40]*Stanford University, Stanford, CA 94305, USA*
[41]*Università di Padova, Dipartimento di Fisica e Astronomia, I-35131 Padova, Italy*
[42]*INFN, Sezione di Padova, I-35131 Padova, Italy*
[43]*CAMK-PAN, 00-716 Warsaw, Poland*
[44]*Astronomical Observatory Warsaw University, 00-478 Warsaw, Poland*
[45]*University of Birmingham, Birmingham B15 2TT, United Kingdom*
[46]*Università degli Studi di Genova, I-16146 Genova, Italy*
[47]*INFN, Sezione di Genova, I-16146 Genova, Italy*
[48]*RRCAT, Indore MP 452013, India*
[49]*Faculty of Physics, Lomonosov Moscow State University, Moscow 119991, Russia*
[50]*SUPA, University of the West of Scotland, Paisley PA1 2BE, United Kingdom*
[51]*University of Western Australia, Crawley, Western Australia 6009, Australia*
[52]*Department of Astrophysics/IMAPP, Radboud University Nijmegen, P.O. Box 9010, 6500 GL Nijmegen, The Netherlands*
[53]*Artemis, Université Côte d'Azur, CNRS, Observatoire Côte d'Azur, CS 34229, Nice cedex 4, France*
[54]*MTA Eötvös University, "Lendulet" Astrophysics Research Group, Budapest 1117, Hungary*
[55]*Institut de Physique de Rennes, CNRS, Université de Rennes 1, F-35042 Rennes, France*
[56]*Washington State University, Pullman, WA 99164, USA*
[57]*Università degli Studi di Urbino 'Carlo Bo', I-61029 Urbino, Italy*
[58]*INFN, Sezione di Firenze, I-50019 Sesto Fiorentino, Firenze, Italy*
[59]*University of Oregon, Eugene, OR 97403, USA*
[60]*Laboratoire Kastler Brossel, UPMC-Sorbonne Universités, CNRS, ENS-PSL Research University, Collège de France, F-75005 Paris, France*
[61]*VU University Amsterdam, 1081 HV Amsterdam, The Netherlands*
[62]*University of Maryland, College Park, MD 20742, USA*
[63]*Center for Relativistic Astrophysics and School of Physics, Georgia Institute of Technology, Atlanta, GA 30332, USA*
[64]*Institut Lumière Matière, Université de Lyon, Université Claude Bernard Lyon 1, UMR CNRS 5306, 69622 Villeurbanne, France*
[65]*Laboratoire des Matériaux Avancés (LMA), IN2P3/CNRS, Université de Lyon, F-69622 Villeurbanne, Lyon, France*
[66]*Universitat de les Illes Balears, IAC3—IEEC, E-07122 Palma de Mallorca, Spain*
[67]*Università di Napoli 'Federico II', Complesso Universitario di Monte S.Angelo, I-80126 Napoli, Italy*
[68]*NASA/Goddard Space Flight Center, Greenbelt, MD 20771, USA*
[69]*Canadian Institute for Theoretical Astrophysics, University of Toronto, Toronto, Ontario M5S 3H8, Canada*
[70]*Tsinghua University, Beijing 100084, China*
[71]*Texas Tech University, Lubbock, TX 79409, USA*
[72]*The Pennsylvania State University, University Park, PA 16802, USA*
[73]*National Tsing Hua University, Hsinchu City, Taiwan 30013, R.O.C.*
[74]*Charles Sturt University, Wagga Wagga, New South Wales 2678, Australia*
[75]*University of Chicago, Chicago, IL 60637, USA*
[76]*Caltech CaRT, Pasadena, CA 91125, USA*
[77]*Korea Institute of Science and Technology Information, Daejeon 305-806, Korea*
[78]*Carleton College, Northfield, MN 55057, USA*
[79]*Università di Roma 'La Sapienza', I-00185 Roma, Italy*
[80]*University of Brussels, Brussels 1050, Belgium*
[81]*Sonoma State University, Rohnert Park, CA 94928, USA*
[82]*Northwestern University, Evanston, IL 60208, USA*
[83]*University of Minnesota, Minneapolis, MN 55455, USA*
[84]*The University of Melbourne, Parkville, Victoria 3010, Australia*
[85]*The University of Texas Rio Grande Valley, Brownsville, TX 78520, USA*
[86]*The University of Sheffield, Sheffield S10 2TN, United Kingdom*
[87]*University of Sannio at Benevento, I-82100 Benevento, Italy and INFN, Sezione di Napoli, I-80100 Napoli, Italy*
[88]*Montclair State University, Montclair, NJ 07043, USA*
[89]*Università di Trento, Dipartimento di Fisica, I-38123 Povo, Trento, Italy*
[90]*INFN, Trento Institute for Fundamental Physics and Applications, I-38123 Povo, Trento, Italy*
[91]*Cardiff University, Cardiff CF24 3AA, United Kingdom*
[92]*National Astronomical Observatory of Japan, 2-21-1 Osawa, Mitaka, Tokyo 181-8588, Japan*
[93]*School of Mathematics, University of Edinburgh, Edinburgh EH9 3FD, United Kingdom*
[94]*Indian Institute of Technology, Gandhinagar Ahmedabad Gujarat 382424, India*
[95]*Institute for Plasma Research, Bhat, Gandhinagar 382428, India*
[96]*University of Szeged, Dóm tér 9, Szeged 6720, Hungary*

[97]Embry-Riddle Aeronautical University, Prescott, AZ 86301, USA
[98]University of Michigan, Ann Arbor, MI 48109, USA
[99]Tata Institute of Fundamental Research, Mumbai 400005, India
[100]American University, Washington, D.C. 20016, USA
[101]University of Massachusetts-Amherst, Amherst, MA 01003, USA
[102]University of Adelaide, Adelaide, South Australia 5005, Australia
[103]West Virginia University, Morgantown, WV 26506, USA
[104]University of Białystok, 15-424 Białystok, Poland
[105]SUPA, University of Strathclyde, Glasgow G1 1XQ, United Kingdom
[106]IISER-TVM, CET Campus, Trivandrum Kerala 695016, India
[107]Institute of Applied Physics, Nizhny Novgorod, 603950, Russia
[108]Pusan National University, Busan 609-735, Korea
[109]Hanyang University, Seoul 133-791, Korea
[110]NCBJ, 05-400 Świerk-Otwock, Poland
[111]IM-PAN, 00-956 Warsaw, Poland
[112]Rochester Institute of Technology, Rochester, NY 14623, USA
[113]Monash University, Victoria 3800, Australia
[114]Seoul National University, Seoul 151-742, Korea
[115]University of Alabama in Huntsville, Huntsville, AL 35899, USA
[116]ESPCI, CNRS, F-75005 Paris, France
[117]Università di Camerino, Dipartimento di Fisica, I-62032 Camerino, Italy
[118]Southern University and A&M College, Baton Rouge, LA 70813, USA
[119]College of William and Mary, Williamsburg, VA 23187, USA
[120]Instituto de Física Teórica, University Estadual Paulista/ICTP South American Institute for Fundamental Research, São Paulo SP 01140-070, Brazil
[121]University of Cambridge, Cambridge CB2 1TN, United Kingdom
[122]IISER-Kolkata, Mohanpur, West Bengal 741252, India
[123]Rutherford Appleton Laboratory, HSIC, Chilton, Didcot, Oxon OX11 0QX, United Kingdom
[124]Whitman College, 345 Boyer Ave, Walla Walla, WA 99362 USA
[125]National Institute for Mathematical Sciences, Daejeon 305-390, Korea
[126]Hobart and William Smith Colleges, Geneva, NY 14456, USA
[127]Janusz Gil Institute of Astronomy, University of Zielona Góra, 65-265 Zielona Góra, Poland
[128]Andrews University, Berrien Springs, MI 49104, USA
[129]Università di Siena, I-53100 Siena, Italy
[130]Trinity University, San Antonio, TX 78212, USA
[131]University of Washington, Seattle, WA 98195, USA
[132]Kenyon College, Gambier, OH 43022, USA
[133]Abilene Christian University, Abilene, TX 79699, USA
[134]Cornell Center for Astrophysics and Planetary Science, Cornell University, Ithaca, New York 14853, USA

(Dated: February 11, 2016)

The LIGO detection of GW150914 provides an unprecedented opportunity to study the two-body motion of a compact-object binary in the large velocity, highly nonlinear regime, and to witness the final merger of the binary and the excitation of uniquely relativistic modes of the gravitational field. We carry out several investigations to determine whether GW150914 is consistent with a binary black-hole merger in general relativity. We find that the final-remnant's mass and spin, determined from the inspiral and post-inspiral phases of the signal, are mutually consistent with the binary black-hole solution in general relativity. The data following the peak of GW150914 are consistent with the least-damped quasi-normal-mode inferred from the mass and spin of the remnant black hole. By using waveform models that allow for parameterized general-relativity violations during the inspiral and merger phases, we perform quantitative tests on the gravitational-wave phase in the dynamical regime and, bound, for the first time several high-order post-Newtonian coefficients. We constrain the graviton Compton wavelength in a hypothetical theory of gravity in which the graviton is massive and place a 90%-confidence lower bound of 10^{13} km. Within our statistical uncertainties, we find no evidence for violations of general relativity in the genuinely strong-field regime of gravity.

Introduction. On September 14, 2015, at 09:50:45 Universal Time, the LIGO detectors at Hanford, Washington and Livingston, Louisiana, detected a gravitational-wave (GW) signal, henceforth GW150914, with an observed signal-to-noise ratio (SNR) ~ 24. The probability that GW150914 was due to a random noise fluctuation was later established to be $< 2\times10^{-7}$ [1, 2]. GW150914 exhibited the expected signature of an inspiral, merger, and ringdown signal from a coalescing binary system [1]. Assuming that general relativity (GR) is the correct description for GW150914, detailed follow-up analyses determined the (detector-frame) component masses of the binary system to be $39^{+6}_{-4}\,M_\odot$ and $32^{+4}_{-5}\,M_\odot$ at 90% credible intervals [3], corroborating the hypothesis that GW150914 was emitted by a binary black hole.

In Newtonian gravity, binary systems move along circular or elliptical orbits with constant orbital period [4, 5]. In GR, binary systems emit GWs [6, 7]; as a consequence, the binary's orbital period decreases over time as energy and angular momentum are radiated away. Electro-magnetic observations of binary pulsars over the four decades since their discovery [8, 9] have made it possible to measure GW-induced orbital-period variations $\dot{P}_{\rm orb} \sim -10^{-14}$–$10^{-12}$, confirming the GW luminosity predicted at leading order in post-Newtonian (PN) theory [10] (i.e., Einstein's quadrupole formula) with exquisite precision [11, 12].

Binary-pulsar observations probe the leading PN corrections to the Newtonian conservative dynamics of binaries, which produce effects such as the relativistic advance of periastron and the Shapiro time delay (see Ref. [12] and references therein). Nevertheless, even in the most relativistic binary pulsar known today, J0737-3039 [11], the orbital period changes at an effectively constant rate. The orbital velocity is $v/c \sim 2 \times 10^{-3}$, and the two neutron stars in the system will coalesce in ~ 85 Myr.

By contrast, GW150914 was emitted by a rapidly evolving, dynamical binary that swept through the detectors' bandwidth and merged in a fraction of a second, with $\dot{P}_{\rm orb}$ ranging from ~ -0.1 at $f_{\rm GW} \sim 30$ Hz to ~ -1 at $f_{\rm GW} \sim 132$ Hz (just before merger, where v/c reached ~ 0.5). Thus, through GW150914 we observe the two-body motion in the large-velocity, highly dynamical, strong-field regime of gravity, leading to the formation of a new merged object, and generating GWs. While Solar-System experiments, binary-pulsar observations, and cosmological measurements are all in excellent agreement with GR (see Refs. [12–14] and references therein), they test it in low-velocity, quasi-static, weak-field, or linear regimes.[1] Thus, GW150914 opens up the distinct opportunity of probing unexplored sectors of GR.

Here we perform several studies of GW150914, aimed at detecting deviations from the predictions of GR. Within the limits set by LIGO's sensitivity and by the nature of GW150914, we find no statistically significant evidence against the hypothesis that, indeed, GW150914 was emitted by a binary system composed of two black holes (i.e., by the Schwarzschild [17] or Kerr [18] GR solutions), that the binary evolved dynamically toward merger, and that it formed a merged rotating black hole consistent with the GR solution.

We begin by constraining the level of coherent (i.e., GW-like) residual strain left after removing the most-probable GR waveform from the GW150914 data, and use it to bound GR violations. We then see that the mass and spin parameters of the final black hole, as predicted from the binary's inspiral signal, are consistent with the final parameters inferred from the post-inspiral (merger and ringdown) signal. We find that the data following the peak of GW150914 are consistent with

[1] While the orbits of binary pulsars are weakly relativistic, pulsars themselves are strongly self-gravitating bodies, so they do offer opportunities to test strong-field gravity [15, 16].

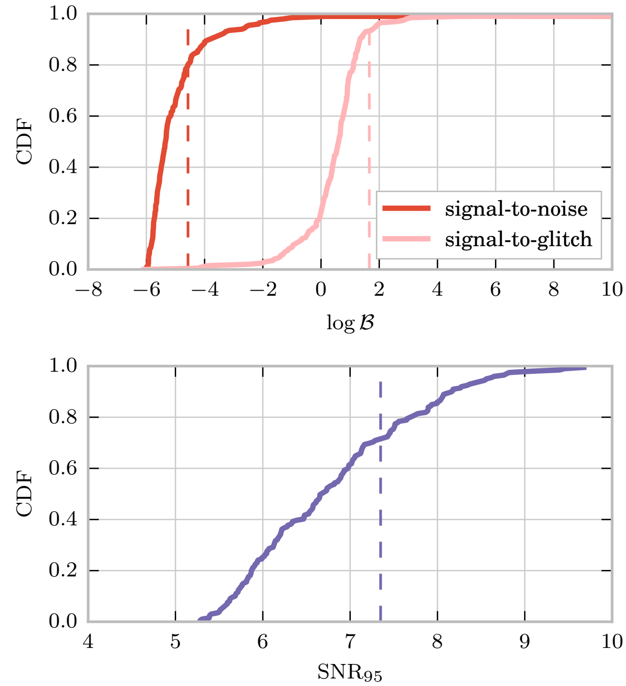

FIG. 1. Upper panel: cumulative distribution function (CDF) of log Bayes factor for the signal-versus-noise and signal-versus-glitch BayesWave models, computed for 100 4-s stretches of data around GW150914. Lower Panel: cumulative distribution function (CDF) of the 95% credible upper bound on network coherent-burst SNR, again computed for 100 instrument-noise segments. In both panels, we indicate with dashed lines the log Bayes factors and upper bound on coherent-burst SNR corresponding to the residuals obtained after subtracting the most-probable waveform from GW150914.

the least-damped quasi-normal-mode (QNM) inferred from the final black-hole characteristics. Next, we perform targeted measurements of the PN and phenomenological coefficients that parameterize theoretical waveform models, and find no tension with the values predicted in GR and numerical-relativity (NR) simulations. Furthermore, we search for evidence of dispersion in the propagation of GW150914 toward the Earth, as it would appear in a theory in which the graviton is assigned a finite Compton wavelength (i.e., a nonzero mass). Finally, we show that, due to the LIGO network configuration, we cannot exclude the presence of non-GR polarization states in GW150914.

Waveform models, systematics and statistical effects. Tests of GR from GW observations build on the knowledge of the gravitational waveform in GR, and the statistical properties of instrumental noise. Any uncontrolled systematic effect from waveform modeling and/or the detectors could in principle affect the outcome of our tests. Thus, we begin by checking that these uncertainties are either below our measurement precision or accounted for.

The analytical waveform models used in this paper were developed within two frameworks: i) the effective-one-body (EOB) formalism [19–23], which combines PN results [10] with NR [24–26] and perturbation theory [27–29], and ii) a phenomenological approach [30–33] based on extending frequency domain PN expressions and hybridizing PN/EOB with NR waveforms. In particular, here we use the double-spin, nonprecessing waveform model developed in Ref. [34], using NR waveforms from Ref. [35], enhanced with reduced-order modeling to speed up waveform generation [36, 37] (henceforth, EOBNR), and the single-effective–spin, precessing waveform model of Refs. [38–40] (henceforth, IMRPhenom).[2] Both models are calibrated against waveforms from direct numerical integration of the Einstein equations.

As shown in Refs. [3, 34, 39, 41, 42], in the region of parameter space relevant for GW150914, the error due to differences between the two analytical waveform models (and between the analytical and numerical-relativity waveforms) is smaller than the typical statistical uncertainty due to the finite SNR of GW150914. To assess potential modeling systematics, we collected existing NR waveforms and generated targeted new simulations [43–48]. The simulations were generated with multiple independent codes, and sample the posterior region for masses and spins inferred for GW150914. To validate the studies below, we added (publicly available and new) NR waveforms as mock signals to the data in the neighbourhood of GW150914 [35, 48]. A further possible cause for systematics are uncertainties in the calibration of the gravitational-strain observable in the LIGO detectors. These uncertainties are modeled and included in the results presented here according to the treatment detailed in Ref. [3].

Residuals after subtracting the most-probable waveform model. The bursts analysis [49], which uses unmodeled templates, can be used to test the consistency of GW150914 with waveform models derived from GR. Using the LALInference [50] Bayesian-inference software library, we identify the most-probable waveform or, equivalently, the *maximum a posteriori* (MAP) binary black-hole waveform [3], compute its effect in the Livingston and Hanford detectors, and then subtract it from the data. If the data are consistent with the theoretical signal, no detectable power should remain after subtraction other than what is consistent with instrumental noise. We analyze the residual with the BayesWaves [51] algorithm developed to characterize generic GW transients. BayesWave uses the evidence ratio (Bayes factor) to rank competing hypotheses given the observed data. We compare predictions from models in which: (i) the data contain only Gaussian noise; (ii) the data contain Gaussian noise and uncorrelated noise transients, or glitches, and (iii) the data contain Gaussian noise and an elliptically polarized GW signal. We compute the signal-to-noise Bayes factor, which is a measure of significance for the excess power in the data, and the signal-to-glitch Bayes factor, which measures the coherence of the excess power between the two detectors. We also apply the same analysis to 100 4-second long segments of data drawn within a few minutes of GW150914, and produce the cumulative distribution functions of Bayes factors shown in Fig. 1. We find that, according to the burst analysis, the GW150914 residual is not statistically distinguishable from the instrumental noise recorded in the vicinity of the detection, suggesting that all of the measured power is well represented by the GR prediction for the signal from a binary black-hole merger. The results of this analysis are very similar regardless of the MAP waveform used (i.e., EOBNR or IMRPhenom).

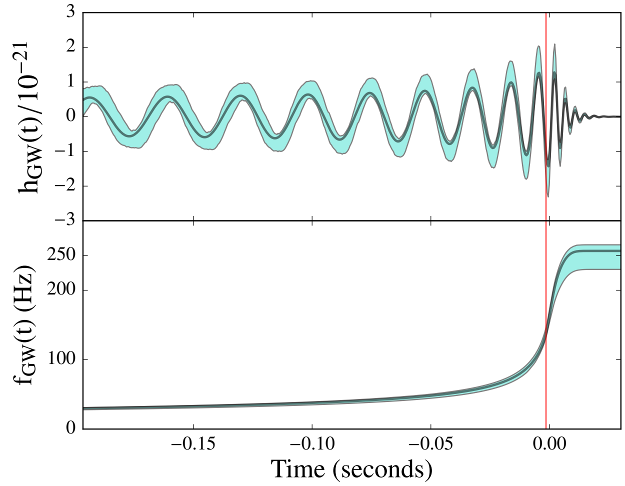

FIG. 2. 90% credible regions for the waveform (upper panel) and GW frequency (lower panel) of GW150914 versus time as estimated by the LALInference analysis [3]. The solid lines in each panel indicate the most probable waveform from GW150914 [3] and its GW frequency. We mark with a vertical line $f_{GW}^{\rm end\,insp} = 132$ Hz, which is used in the IMR consistency test to delineate the boundary between the inspiral and post-inspiral parts.

We compute the 95% upper bound on the coherent network $\mathrm{SNR}_{\rm res}$ identified by the unmodeled-burst search in the GW150914 residual after subtracting the MAP waveform. This upper bound is $\mathrm{SNR}_{\rm res} \leq 7.3$ at 95% confidence, independently of the MAP waveform used (i.e., EOBNR or IMRPhenom). We note that this unmodeled-burst SNR has a different meaning compared to the (modeled) matched-filtering binary-coalescence SNR of 24 cited for GW150914. Indeed, the upper-limit $\mathrm{SNR}_{\rm res}$ inferred for GW150914 lies in the typical range for the data segments around GW150914 (see the bottom panel of Fig. 1), so it can be attributed to instrument noise alone.

If we assume that $\mathrm{SNR}_{\rm res}$ is entirely due to the mismatch between the MAP waveform and the underlying true signal, and that the putative violation of GR cannot be reabsorbed in the waveform model by biasing the estimates of the physical parameters [52, 53], we can constrain the minimum *fitting factor* (FF) [54] between the MAP model and GW150914. An imperfect fit to the data leaves $\mathrm{SNR}_{\rm res}^2 = (1 - \mathrm{FF}^2)\,\mathrm{FF}^{-2}\,\mathrm{SNR}_{\rm det}^2$ [55, 56] where $\mathrm{SNR}_{\rm det} = 25.3^{+0.1}_{-0.2}$ is the network SNR inferred by LALInference [3]. $\mathrm{SNR}_{\rm res} \leq 7.3$ then implies $\mathrm{FF} \geq 0.96$.

[2] The specific names of the two waveform models that we use in the LIGO Algorithm Library are SEOBNRv2_ROM_DoubleSpin and IMRPhenomPv2.

Considering that, for parameters similar to those inferred for GW150914, our waveform models have much higher FFs against numerical GR waveforms, we conclude that the noise-weighted correlation between the observed strain signal and the true GR waveform is $\geq 96\%$. This statement can be read as implying that the GR prediction for GW150914 is verified to better than 4%, in a precise sense related to noise-weighted signal correlation; and conversely, that effects due to GR-violations in GW150914 are limited to less than 4% (for effects that cannot be reabsorbed in a redefinition of physical parameters).

Inspiral, merger and ringdown consistency test. We now perform a test to show that the inspiral and merger/ringdown parts of GW150914 do not deviate from the predictions of a binary black-hole coalescence in GR. One way to do that is to compare the estimates of the mass and spin of the remnant obtained from different parts of the waveform, using the relations between the binary's components and final masses and spins provided by NR [57].

We first explore the posterior distributions of the binary's component masses and spins from the "inspiral" (low-frequency) part of the observed signal, using the nested sampling algorithm from the LALInference software library [50], and then use formulae obtained from NR simulations to get posterior distributions of the remnant's mass and spin. The inspiral part of the signal is defined as follows. We fix the frequency at which the inspiral phase ends to $f_{\rm GW}^{\rm end\,insp} = 132$ Hz, close to the MAP waveform's merger frequency [3] (see Figs. 2 and 5 below), and restrict the waveform model in the frequency domain from 20 Hz to $f_{\rm GW}^{\rm end\,insp}$. Next, we estimate posterior distributions on the mass and spin of the final compact object from the "post-inspiral" (high-frequency) signal that is dominated by the contribution from merger and ringdown stages (i.e., from the waveform model that extends from $f_{\rm GW}^{\rm end\,insp}$ up to 1024 Hz), again using formulae obtained from NR simulations. We notice that the expectation value of the $\mathrm{SNR_{det}}$ from the MAP waveform whose support is only from 20 Hz to 132 Hz is ~ 19.5, while when the support is from 132 Hz to 1024 Hz it is ~ 16. Finally, we compare these two estimates of the final M_f and dimensionless spin a_f, and compare them also against the estimate performed using the full inspiral–merger–ringdown waveform GW150914. In all cases, we average the posteriors obtained with the EOBNR and IMRPhenom waveform models, following the procedure outlined in Ref. [3]. Technical details about the implementation of this test can be found in Ref. [58].

This test is similar in spirit to the χ^2 GW-search veto [2, 59] that penalizes event candidates if their (noise-weighted) residual with respect to theoretical templates is too uneven across frequency segments—a warning that some parts of the waveform are fit much worse than others, and thus the candidates may be due to instrument glitches that are very loud, but do not resemble binary-inspiral signals. However, χ^2 tests are performed by comparing the data with a single theoretical waveform, while in this case we allow the inspiral and

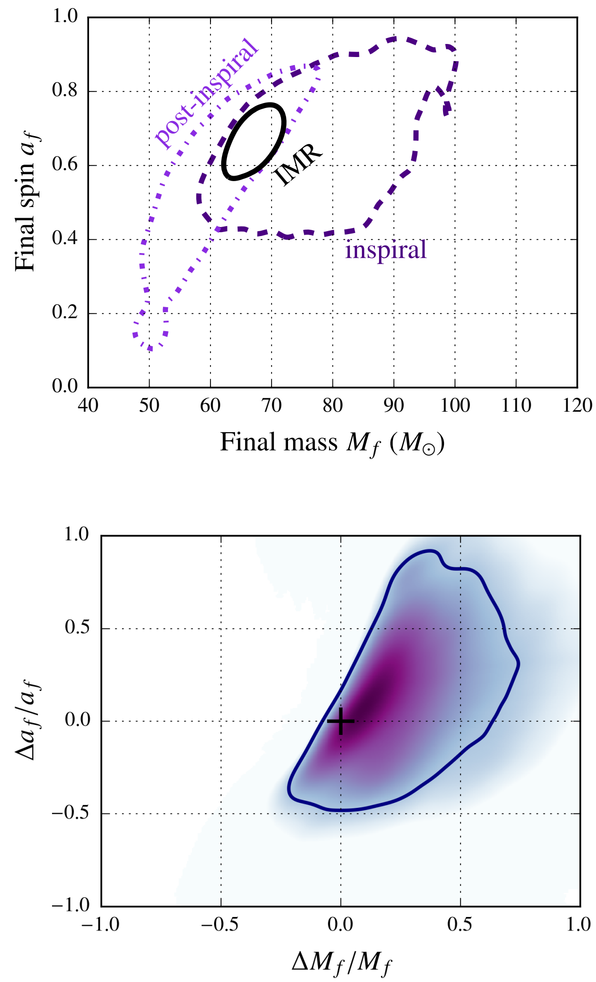

FIG. 3. *Top panel*: 90% confidence regions on the joint posterior distributions for the mass M_f and dimensionless spin a_f of the final compact object predicted from the inspiral (dark violet, dashed) and measured from the post-inspiral (violet, dot-dashed), as well as the result from a full inspiral-merger-ringdown (IMR) analysis (black). *Bottom panel*: Posterior distributions for the parameters $\Delta M_f/M_f$ and $\Delta a_f/a_f$ that describe the fractional difference in the estimates of the final mass and spin from inspiral and post-inspiral parts. The contour shows the 90% confidence region. The plus symbol indicates the expected value $(0, 0)$ in GR.

merger/ringdown partial waveforms to select different physical parameters. Thus, this test should be sensitive to subtler deviations from the predictions of GR.

In Fig. 2 we show the EOBNR MAP waveform [3] with its instantaneous GW frequency; the shaded areas correspond to the 90% credible regions. The vertical line marks $f_{\rm GW}^{\rm end\,insp} = 132$ Hz; see also Fig. 5 below, where we plot the MAP frequency-domain amplitude and indicate the inspiral, intermediate, and merger-ringdown regimes. In Fig. 3 we summarize our findings. The top panel of Fig. 3 shows the posterior distributions of M_f and a_f estimated from the inspiral and post-inspiral parts, as well as from the entire inspiral–merger–

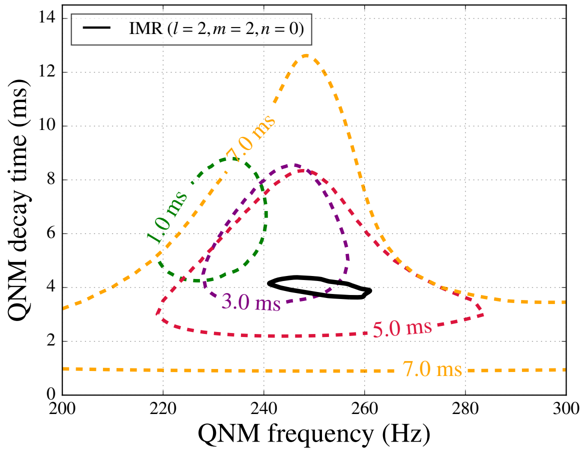

FIG. 4. We show the posterior 90% confidence regions from Bayesian parameter estimation for a damped-sinusoid model, assuming different start-times $t_0 = t_M + 1, 3, 5, 7$ ms, labeled by offset from the merger time t_M of the most-probable waveform from GW150914. The black solid line shows contours of 90% confidence region for the frequency f_0 and decay time τ of the $\ell = 2$, $m = 2$ and $n = 0$ (i.e., the least damped) QNM obtained from the inspiral-merger-ringdown waveform for the entire detector's bandwidth.

ringdown signal. It confirms the expected behavior: the intersection of the inspiral and post-inspiral 90% confidence regions (defined by the isoprobability contours that enclose 90% of the posterior) contain the inspiral-merger-ringdown 90% confidence region. We have verified that these conclusions are not affected by the specific formula [38, 57, 60] used to predict M_f and a_f, nor by the choice of $f_{\rm GW}^{\rm end\,insp}$ within a few cycles of the waveform's peak.

To assess the significance of our findings more quantitatively, we define parameters $\Delta M_f/M_f$ and $\Delta a_f/a_f$ that describe the fractional difference in the two estimates of the final mass and spin [58]. In the bottom panel of Fig. 3 we show their joint posterior distribution; the solid line marks the isoprobability contour that contains 90% of the posterior. The plus symbol indicates the null $(0, 0)$ result expected in GR, which lies on the isoprobability contour that encloses 28% of the posterior. We have checked that when performing analyses of NR signals added to LIGO instrumental noise, the null $(0, 0)$ result expected in GR lies within isoprobability contours that encloses 68% of the posterior, roughly 68% of the time, as expected from random-noise fluctuations. By contrast, our test can rule out the null hypothesis (with high statistical significance) when analyzing a simulated signal that reflects a significant GR violation in the frequency dependence of the energy and angular-momentum loss [58], even when we choose violations which would be too small to be noticeable in double-pulsar observations [12]. Thus, our inspiral-merger-ringdown test shows no evidence of discrepancies with the predictions of GR.

The mass and dimensionless spin of the final black hole implied by formulae obtained from NR simulations together with the component mass and spin posteriors [3] are $67^{+4}_{-4}\,M_\odot$ (in the source frame $62^{+4}_{-4}\,M_\odot$) and $0.67^{+0.05}_{-0.07}$ at 90% confidence. From the posterior distributions of the mass and spin of the final black hole, we can predict the frequency and decay time of the least-damped QNM (i.e., the $\ell = 2, m = 2, n = 0$ overtone) [61]. We find $f_{220}^{\rm QNM} = 251^{+8}_{-8}$ Hz and $\tau_{220}^{\rm QNM} = 4.0^{+0.3}_{-0.3}$ ms at 90% confidence.

Testing for the least-damped QNM in the data. We perform a test to check the consistency of the data with the predicted least-damped QNM of the remnant black hole. For this purpose we compute the Bayes factor between a damped-sinusoid waveform model and Gaussian noise, and estimate the corresponding parameter posteriors. The signal model used is $h(t \geq t_0) = A\, e^{-(t-t_0)/\tau} \cos[2\pi f_0 (t - t_0) + \phi_0]$, $h(t < t_0) = 0$, with fixed starting time t_0, and uniform priors over the unknown frequency $f_0 \in [200, 300]$ Hz and damping time $\tau \in [0.5, 20]$ ms. The prior on amplitude A and phase ϕ_0 is chosen as a two-dimensional Gaussian isotropic prior in $\{A_s \equiv -A \sin\phi_0,\ A_c \equiv A\cos\phi_0\}$ with a characteristic scale H, which is in turn marginalized over the range $H \in [2, 10] \times 10^{-22}$ with a prior $\propto 1/H$. This is a practical choice that encodes relative ignorance about the detectable damped-sinusoid amplitude in this range.

We compute the Bayes factor and posterior estimates of $\{f_0, \tau\}$ as a function of the unknown QNM start-time t_0, which we parameterize as an offset from a fiducial GPS merger time[3] $t_{\rm M} = 1126259462.423$ (referring to the GPS arrival time at the LIGO Hanford site). Figure 4 shows various different posterior 90% credible contours in $\{f_0, \tau\}$ as a function of the start-time offset $t_0 - t_{\rm M}$ from merger, in addition to the least-damped QNM prediction from GR derived in the previous section.

The 90% posterior contour starts to overlap the GR prediction from the IMR waveform at $t_0 = t_{\rm M} + 3$ ms, or $\sim 10\,M$ after merger. The corresponding Bayes factor at this point is $\log_{10} B \sim 17$ with an SNR in the MAP waveform $\{f_0, \tau\}$ of SNR ~ 9. At $t_0 = t_{\rm M} + 5$ ms the MAP waveform actually falls within the (much smaller) IMR prediction uncertainty, and the Bayes factor is $\log_{10} B \sim 9$ and SNR ~ 7. At $t_0 = t_{\rm M} + 7$ ms, or about $20\,M$ after merger, the posterior uncertainty becomes quite large, and the Bayes factor drops to $\log_{10} B \sim 2.6$ with SNR ~ 4.4. The signal becomes undetectable shortly thereafter, $t_0 \geq t_{\rm M} + 8$ ms or so, where $B \sim 1$.

Measuring only the frequency and decay time of *one* damped sinusoid in the data does not allow us to conclude that we have observed the least-damped QNM of the final black hole. The measured quality factor can be obtained from several QNMs that have different black-hole's spin, harmonics and overtones (see, e.g., Ref. [61] and references therein). However, the overlap between the 90% posterior contour of the damped-sinusoid waveform model and the 90% confidence region estimated from the IMR waveform indicates that

[3] The merger time is obtained by taking the EOBNR MAP waveform and lining this waveform up with the data such that the largest SNR is obtained. The merger time is then defined as the point at which the quadrature sum of the h_+ and $h_\times$ polarizations is maximum.

the data are consistent with the presence of the least-damped QNM as predicted by GR, occurring between 10–20M after merger [62–64]. In the future, we will extend the analysis to two damped sinusoids and explore the possibility of independently extracting the final black hole's mass and spin. A test of the general relativistic no-hair theorem [65, 66] requires the identification of at least two QNM frequencies in the ringdown waveform [67–69]. Moreover, the independent determination of the remnant mass and spin will allow us to test the second law of black-hole dynamics [70, 71].

Constraining parameterized deviations from general-relativistic inspiral–merger–ringdown waveforms. Because GW150914 was emitted by a binary black hole in its final phase of rapid orbital evolution, its gravitational phasing (or phase evolution) encodes nonlinear conservative and dissipative effects that are not observable in binary pulsars, whose orbital period changes at an approximately constant rate. [4] Those effects include tails of radiation due to backscattering of GWs by the curved background around the coalescing black holes [72], non-linear tails (i.e., tails of tails) [73], couplings between black-hole spins and the binary's orbital angular momentum, interactions between the spins of the two bodies [74–76], and excitations of QNMs [27–29] as the remnant black hole settles in the stationary configuration.

Whether all these subtle effects can actually be identified in GW150914 and tested against GR predictions depends of course on their strength with respect to instrument noise and on whether the available waveform models are parameterized in terms of those physical effects. GW150914 is moderately loud, with SNR ~ 24, certainly much smaller than what can be achieved in binary-pulsar observations. Our ability to analyze the fine structure of the GW150914 waveform is correspondingly limited. Our approach is to adopt a parameterized analytical family of inspiral–merger–ringdown waveforms, then treat the waveform coefficients as free variables that can be estimated (either individually or in groups) from the GW150914 data [77–82]. We can then verify that the posterior probability distributions for the coefficients include their GR values.

The simplest and fastest parameterized waveform model that is currently available [39] can be used to bound physical effects only for the coefficients that enter the early inspiral phase, because for the late inspiral, merger and ringdown phases it uses phenomenological coefficients fitted to NR waveforms. Louder GW events, to be collected as detector sensitivity improves, and more sophisticated parameterized waveform models, will allow us to do much more stringent and physical tests targeted at specific relativistic effects. We work within a subset of the TIGER framework [82, 83] and perform a null-hypothesis test by comparing GW150914 with a *generalized*, analytical inspiral–merger–ringdown waveform model (henceforth, gIMR) that

[4] Current binary-pulsar observations do constrain conservative dynamics at 1PN order and they partially constrain spin–orbit effects at 1.5PN order through geodetic spin precession [12].

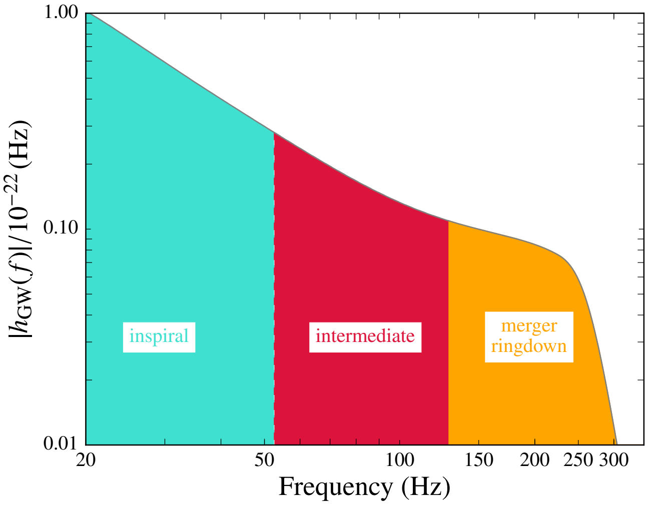

FIG. 5. Frequency regions of the parameterized waveform model as defined in the text and in Ref. [39]. The plot shows the absolute value of the frequency-domain amplitude of the most-probable waveform from GW150914 [3]. The inspiral region (cyan) from 20 Hz to ∼55 Hz corresponds to the early and late inspiral regimes. The intermediate region (red) goes from ∼ 55 Hz to ∼ 130 Hz. Finally, the merger-ringdown region (orange) goes from ∼ 130 Hz to the end of the waveform.

includes parameterized deformations with respect to GR. In this framework, deviations from GR are modeled as *fractional changes* $\{\delta\hat{p}_i\}$ in any of the parameters $\{p_i\}$ that parameterize the GW phase expression in the baseline waveform model. Similarly to Refs. [82, 83], we only consider deviations from GR in the GW phase, while we leave the GW amplitude unperturbed. Indeed, at the SNR of GW150914 (i.e., SNR ~ 24), we expect to have much higher sensitivity to the GW phase rather than to its amplitude. Also, amplitude deviations could be reabsorbed in the calibration error model used to analyse GW150914 [3].

We construct gIMR starting from the frequency-domain IMRPhenom waveform model. The dynamical stages that characterize the coalescence process can be represented in the frequency-domain by plotting the absolute value of the waveform's amplitude. We review those stages in Fig. 5 to guide the reader towards the interpretation of the results that are summarized in Table I and Figs. 6 and 7. We refer to the *early-inspiral stage* as the PN part of the GW phase. This stage of the phase is known analytically up to $(v/c)^7$ and it is parameterized in terms of the PN coefficients φ_j, $j = 0, \ldots, 7$ and the *logarithmic* terms φ_{jl}, $j = 5, 6$. The *late-inspiral stage*, parameterized in terms of σ_j, $j = 1, \ldots, 4$, is defined as the phenomenological extension of the PN series to $(v/c)^{11}$. The *early* and *late inspiral* stages are denoted simply as *inspiral* both in Ref. [39] and in Fig. 5. The *intermediate stage* that models the transition between the inspiral and the merger-ringdown phase is parameterized in terms of the phenomenological coefficients β_j, $j = 1, 2, 3$. Finally, the *merger–ringdown* phase is parameterized in terms of the phenomenological coeffi-

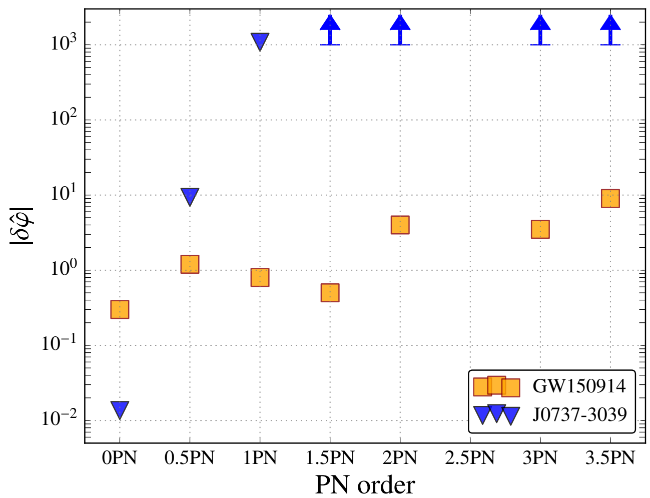

FIG. 6. 90% upper bounds on the fractional variations for the known PN coefficients compared to their known value in GR. The orange squares are the 90% upper bounds obtained from the single-parameter analysis of GW150914. As a comparison, the blue triangles show the 90% upper bounds extrapolated exclusively from the orbital-period derivative, $\dot{P}_{\rm orb}$, of the double pulsar J0737-3039 [12, 84]. The GW phase deduced from an almost constant $\dot{P}_{\rm orb}$ cannot provide significant information as the PN order is increased. As an illustration of the different dynamical regimes between the double pulsar and GW150914, we show the bounds for the former only up to 1PN order. We do not report on the 2.5PN coefficient because, being degenerate with the reference phase, it is unmeasurable. We also do not report on the logarithmic terms in the PN series at 2.5PN and 3PN order, which can be found in Table I and in Fig. 7.

cients α_j, $j = 1, 2, 3$. Due to the procedure through which the model is constructed, which involves fitting a waveform phasing ansatz to a calibration set of EOB joined to NR waveforms [39], there is an intrinsic uncertainty in the values of the phenomenological parameters of the IMRPhenom model. For the intermediate and merger-ringdown regime, we verified that these intrinsic uncertainties are much smaller than the corresponding statistical uncertainties for GW150914 and thus do not affect our conclusions. In the late-inspiral case, the uncertainties associated with the calibration of the σ_j parameters are very large and almost comparable with our results. Therefore, we do not report results for the σ_j parameters.

As said, we construct the gIMR model by introducing (fractional) deformations, $\delta\hat{p}_i$, for each of the IMRPhenom phase parameters p_i, which appear in the different stages of the coalescence discussed above. At each point in parameter space, the coefficients p_i are evaluated for the local physical parameters (masses, spins) and multiplied by factors $(1 + \delta\hat{p}_i)$. In this parameterization, GR is uniquely defined as the locus in the parameter space where each of the phenomenological parameters, $\{\delta\hat{p}_i\}$, assumes exactly the value of zero. In summary, our battery of testing parameters consists of: (i) early-inspiral stage: $\{\delta\hat{\varphi}_0, \delta\hat{\varphi}_1, \delta\hat{\varphi}_2, \delta\hat{\varphi}_3, \delta\hat{\varphi}_4, \delta\hat{\varphi}_{5l}, \delta\hat{\varphi}_6, \delta\hat{\varphi}_{6l}, \delta\hat{\varphi}_7\}$ [5], (ii) late-inspiral stage: $\{\delta\hat{\sigma}_2, \delta\hat{\sigma}_3, \delta\hat{\sigma}_4\}$, (iii) intermediate regime: $\{\delta\hat{\beta}_2, \delta\hat{\beta}_3\}$, and (iv) merger-ringdown regime: $\{\delta\hat{\alpha}_2, \delta\hat{\alpha}_3, \delta\hat{\alpha}_4\}$. We do not consider parameters that are degenerate with either the reference time or the reference phase. For our analysis, we explore two scenarios: *single-parameter* analysis, in which only one of the parameters is allowed to vary while the remaining ones are fixed to their GR value, that is zero, and *multiple-parameter* analysis in which all parameters in each stage are allowed to vary simultaneously.

The rationale behind our choices of single- and multiple-parameter analyses comes from the following considerations. In most known alternative theories of gravity [13, 14, 85], the corrections to GR extend to all PN orders even if in most cases they have been computed only at leading PN order. Considering that GW150914 is an inspiral, merger and ringdown signal, sweeping through the detector between 20 Hz and 300 Hz, we expect to see the signal deviations from GR at all PN orders. The single-parameter analysis corresponds to minimally extended models, that can capture deviations from GR that predominantly, but not only, occur at a specific PN order. Due to their covariance, we find that in the multiple-parameter analysis the correlations among the parameters is very significant. In other words, a shift in one of the testing parameters can always be compensated by an opposite sign change of another parameter and still return the same overall GW phase. Thus, it is not surprising that the multiple-parameter case provides a much more conservative statement on the agreement between GW150914 and GR.

For each set of testing parameters, we perform a separate LALInference analysis, where in concert with the full set of GR parameters [3], we also explore the posterior distributions for the specified set of testing parameters. Since our testing parameters are purely phenomenological (except the ones of the PN early-inspiral stage), we choose their prior probability distributions to be uniform and wide enough to encompass the full posterior probability density function in the single-parameter case. In particular we employ: $\delta\hat{\varphi}_i \in [-20, 20]$; $\delta\hat{\sigma}_i \in [-30, 30]$; $\delta\hat{\beta}_i \in [-3, 3]$; $\delta\hat{\alpha}_i \in [-5, 5]$. In all the analyses that we performed we obtain estimates of the physical parameters — e.g., masses and spins – that are in agreement with the ones reported in Ref. [3].

We show in Fig. 6 the 90% upper bounds on the values of the (known) PN parameters $\delta\hat{\varphi}_i$ with $i = 0, \ldots, 7$ (except for i = 5, which is degenerate with the reference phase), when varying the testing parameters one at the time, keeping the other parameters fixed to the GR value. As an illustration, following Ref. [84], we also show in Fig. 6 the bounds obtained from the orbital-period derivative $\dot{P}_{\rm orb}$ of the double pulsar J0737-3039 [12]. Not surprisingly, since in binary pulsars the orbital period changes at essentially a constant rate, the corresponding bounds quickly become rather loose as the PN or-

[5] Unlike Ref. [39], we explicitly include the logarithmic terms $\delta\hat{\varphi}_{5l}$ and $\delta\hat{\varphi}_{6l}$. We also include the 0.5PN parameter that is zero in GR, thus $\delta\hat{\varphi}_1$ is an absolute shift rather than relative.

TABLE I. Summary of the results for gIMR. For each parameter in the gIMR model, we report its frequency dependence, median and 90% credible regions, the quantile for the GR value of 0 from the 1D posterior probability density function. Finally, the last two columns show log Bayes factors in base 10 between GR and the gIMR model. The uncertainties on the log Bayes factors are 2σ. The a and b in $\delta\hat{\alpha}_4$ are functions of the component masses and spins (see Ref. [39]). For each field, we report the corresponding quantities for both the single-parameter and multiple-parameter analyses.

waveform regime			median		GR quantile		$\log_{10} B^{\rm GR}_{\rm model}$	
	parameter	$f-$dependence	single	multiple	single	multiple	single	multiple
early-inspiral regime	$\delta\hat{\varphi}_0$	$f^{-5/3}$	$-0.1^{+0.1}_{-0.1}$	$1.3^{+3.0}_{-3.2}$	0.94	0.30	1.9 ± 0.2	3.7 ± 0.6
	$\delta\hat{\varphi}_1$	$f^{-4/3}$	$0.3^{+0.4}_{-0.4}$	$-0.5^{+0.6}_{-0.6}$	0.16	0.93	1.6 ± 0.2	
	$\delta\hat{\varphi}_2$	f^{-1}	$-0.4^{+0.3}_{-0.4}$	$-1.6^{+18.8}_{-16.6}$	0.96	0.56	1.2 ± 0.2	
	$\delta\hat{\varphi}_3$	$f^{-2/3}$	$0.2^{+0.2}_{-0.2}$	$2.0^{+13.4}_{-13.9}$	0.02	0.42	1.2 ± 0.2	
	$\delta\hat{\varphi}_4$	$f^{-1/3}$	$-1.9^{+1.6}_{-1.7}$	$-1.9^{+19.3}_{-16.4}$	0.98	0.56	0.3 ± 0.2	
	$\delta\hat{\varphi}_{5l}$	$\log(f)$	$0.8^{+0.5}_{-0.6}$	$-1.4^{+18.6}_{-16.9}$	0.01	0.55	0.7 ± 0.4	
	$\delta\hat{\varphi}_6$	$f^{1/3}$	$-1.4^{+1.1}_{-1.1}$	$1.2^{+16.8}_{-18.9}$	0.99	0.47	0.4 ± 0.2	
	$\delta\hat{\varphi}_{6l}$	$f^{1/3}\log(f)$	$8.9^{+6.8}_{-6.8}$	$-1.9^{+19.1}_{-16.1}$	0.02	0.57	-0.3 ± 0.2	
	$\delta\hat{\varphi}_7$	$f^{2/3}$	$3.8^{+2.9}_{-2.9}$	$3.2^{+15.1}_{-19.2}$	0.02	0.41	-0.0 ± 0.2	
intermediate regime	$\delta\hat{\beta}_2$	$\log f$	$0.1^{+0.4}_{-0.3}$	$0.2^{+0.6}_{-0.5}$	0.24	0.28	1.4 ± 0.2	2.3 ± 0.2
	$\delta\hat{\beta}_3$	f^{-3}	$0.1^{+0.6}_{-0.3}$	$-0.0^{+0.8}_{-0.7}$	0.31	0.56	1.2 ± 0.4	
merger-ringdown regime	$\delta\hat{\alpha}_2$	f^{-1}	$-0.1^{+0.4}_{-0.4}$	$0.0^{+1.0}_{-1.2}$	0.68	0.50	1.2 ± 0.2	2.1 ± 0.4
	$\delta\hat{\alpha}_3$	$f^{3/4}$	$-0.3^{+1.9}_{-1.5}$	$0.0^{+4.4}_{-4.4}$	0.60	0.51	0.7 ± 0.2	
	$\delta\hat{\alpha}_4$	$\tan^{-1}(af+b)$	$-0.1^{+0.5}_{-0.5}$	$-0.1^{+1.1}_{-1.0}$	0.68	0.62	1.1 ± 0.2	

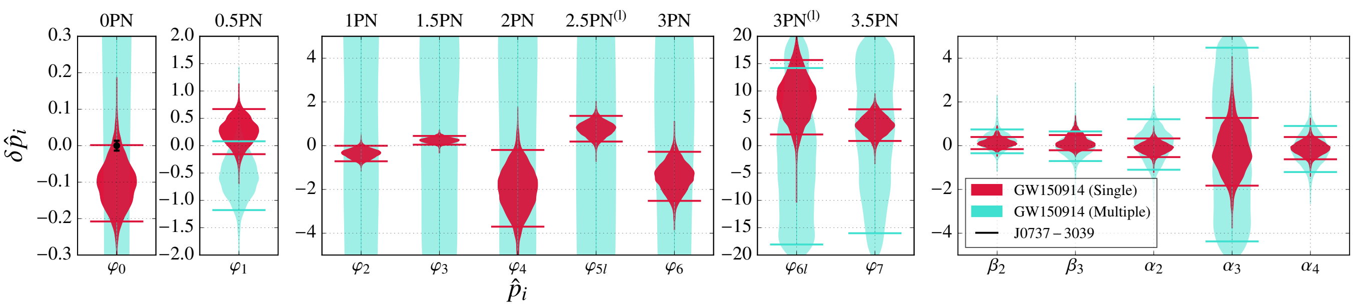

FIG. 7. *Violin* plot summarizing the posterior probability density distributions for all the parameters in the gIMR model. From left to right: the plot shows increasingly high-frequency regimes as outlined in the text and Fig. 5; the leftmost posteriors, labeled from 0PN to 3.5PN, are for the early-inspiral PN regime; the β_i and α_i parameters correspond to the intermediate and merger-ringdown regimes. Note that the constraints get tighter in the merger and ringdown regimes. In red, we show posterior probability distributions for the single-parameter analysis while in cyan we show the posterior distribution for the multiple-parameter analysis. The black error bar at 0PN show the bound inferred from the double pulsar; higher PN orders are not shown as their constraints are far weaker than GW150914's measurement and they would appear in the plot as vertical black lines covering the entire y-axis. Summary statistics are reported in Table I. The 2.5PN term reported in the figure refers to the logarithmic term $\delta\hat{\varphi}_{5l}$. Because of their very different scale compared to the rest of the parameters, the 0PN and 0.5PN order posterior distributions from GW150914 and the double-pulsar limits at 0PN order are shown on separate panels. The error bars indicate the symmetric 90% credible regions reported in Table I. Due to correlations among parameters, the posterior distribution obtained from the multiple-parameter analyses in the early-inspiral regimes are informative only for the 0.5PN coefficient.

der is increased. As a consequence, the double-pulsar bounds are significantly less informative than GW150914, except at 0PN order, where the double-pulsar bound is better thanks to the long observation time ($\sim$ 10 years against $\sim$ 0.4 s for GW150914's). [6] Thus, GW150914 allows us for the first time to constrain the coefficients in the PN series of the phasing up to 3.5PN order.

Furthermore, in Table I and Fig. 7 we summarize the constraints on each testing parameter $\delta\hat{\varphi}_i$ for the single and multiple-parameter analyses. In particular, in the 6th and 7th columns of Table I, we list the quantile at which the GR value of zero is found within the marginalised 1-dimensional pos-

[6] We note that when computing the upper bounds with the binary-pulsar observations, we include the effect of eccentricity only in the 0PN parameter. For the higher PN parameters, the effect is not essential considering that the bounds are not very tight.

terior. We note that in the single-parameter analysis, for several parameters, the GR value is found at quantiles close to an equivalent of 2–2.5σ, i.e., close to the tails of their posterior probability functions. The fact that for the majority of the early-inspiral parameters the GR value lies in the tails of their posteriors, is not surprising since we find that these parameters have a substantial degree of correlation. Thus, if a particular noise realization causes the posterior distribution of one parameter to be off-centered with respect to zero, we expect that the posteriors of all the other parameters to be also off-centered. This is indeed what we observe. The medians for the early-inspiral single-parameter posteriors reported in Table I show opposite sign shifts that follow closely the sign pattern found in the PN series.

We repeated our single-parameter analysis on 20 datasets obtained by adding NR waveforms with GW150914-like parameters to noise-only data segments close to GW150914. In one instance, we observed $\delta\hat{\varphi}_i$ posterior distribution very similar to those of Table I and Fig. 7. Thus, it is not unlikely that instrumental noise fluctuations would cause the degree of apparent deviation from GR found to occur in the single-parameter quantiles for GW150914, even in the absence of an actual deviation from GR. However, we cannot fully exclude a systematic origin from inaccuracies or even missing physics in our waveform models. Future observations will shed light on this aspect.

In the multiple-parameter analyses, which account for correlations between parameters, GR is usually found to be very close to the median of the distribution. This is partly due to the fact that we are not sensitive to most of the early-inspiral parameters, with the exception of the 0PN and 0.5PN coefficients. As for the intermediate and merger-ringdown parameters, since most of the SNR for GW150914 comes from the high-frequency portion of the observed signal, we find that the constraints on those coefficients are very robust and essentially independent of the analysis configuration chosen, single or multiple.

Finally, the last two columns of Table I report the logarithm of the ratio of the marginal likelihoods (the logarithm of the Bayes factor $\log_{10} B^{\rm GR}_{\rm model}$) as a measure of the relative goodness-of-fit between the IMRPhenom and gIMR models (see Ref. [3] and references therein). If $\log_{10} B^{\rm GR}_{\rm model} < 0\,(> 0)$ then GR fits the data worse (better) than the competing model. The uncertainty over $\log_{10} B^{\rm GR}_{\rm model}$ is estimated by running several independent instances of LALInference. The $\log_{10} B^{\rm GR}_{\rm model}$ corroborates our findings that GW150914 provides no evidence in favor of the hypothesis that GR is violated.[7]

[7] Because of the normalization of the prior probability distributions, the Bayes factors include a penalty factor — the so-called Occam factor — for models that have more parameters. The wider the prior range, the more severe the penalization. Therefore, different choices for $\delta\hat{p}_i$ would lead to different numerical values of $\log_{10} B^{\rm GR}_{\rm model}$. To establish the significance of the Bayes factors, validation analyses [82, 83] would be necessary and will be presented in forthcoming studies.

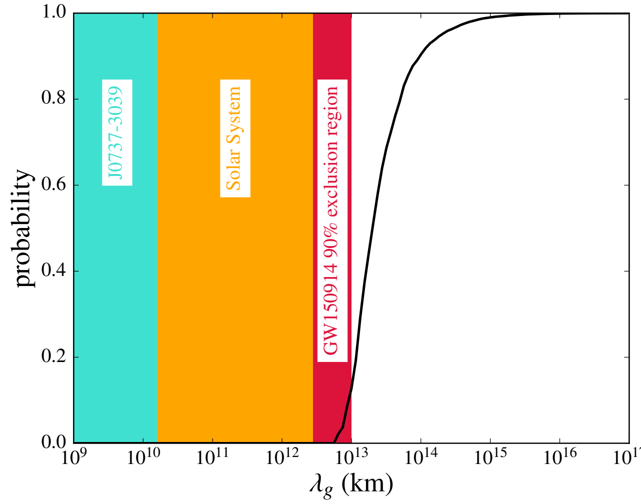

FIG. 8. Cumulative posterior probability distribution for λ_g (black curve) and exclusion regions for the graviton Compton wavelength λ_g from GW150914. The shaded areas show exclusion regions from the double pulsar observations (turquoise), the static Solar System bound (orange) and the 90% (crimson) region from GW150914.

Constraining the graviton Compton wavelength. Since the 1970s, there have been attempts to construct theories of gravity mediated by a graviton with a non-zero mass. Those attempts have led to conceptual difficulties, some of which have been addressed, circumvented or overcome, but others remain open (see Ref. [86] and references therein). Here, we take a phenomenological approach and consider a hypothetical massive-graviton theory in which, due to a modification of the dispersion relation, GWs travel at a speed different from the speed of light.

In GR, gravitons are massless and travel at the speed of light $v_g = c$. In a hypothetical massive graviton theory the dispersion relation can be modified to $E^2 = p^2c^2 + m_g^2c^4$ where E is the graviton energy, p the momentum, and m_g is the graviton rest mass related to the graviton Compton wavelength as $\lambda_g = h/(m_g c)$ with h the Planck constant. Thus, we have $v_g^2/c^2 \equiv c^2p^2/E^2 = 1 - h^2c^2/(\lambda_g^2 E^2)$, and the massive graviton propagates at an energy (or frequency) dependent speed. In such a massive graviton theory the Newtonian potential is altered by a Yukawa-type correction: $\varphi(r) = (GM/r)[1 - \exp(-r/\lambda_g)]$. Bounds that do not probe the propagation of gravitational interactions when λ_g is finite (i.e., the so-called *static* bounds) from Solar System observations [87, 88], model-dependent large-scale dynamics of galactic clusters [89] and model-dependent weak lensing observations [90] are 2.8×10^{12} km, 6.2×10^{19} km and 1.8×10^{22} km, respectively. The only *dynamical bound* to date comes from the binary-pulsar observations [91] and it is $\lambda_g > 1.6 \times 10^{10}$ km. If the Compton wavelength of gravitons is finite, then lower frequencies propagate slower compared to higher frequencies, and this dispersion of the waves can be incorporated in the gravitational phasing from a coalescing binary. In particular, neglecting all possible effects on the binary dynamics that could be introduced by the massive graviton theory, Ref. [88] found that the phase term $\Phi_{\rm MG}(f) = -(\pi D c)/[\lambda_g^2(1+z)f]$ (formally a 1PN order term) should be added to the overall GW phase. In this expression, z is the cosmological redshift and D is a cosmological distance defined in Eq. (2.5) of Ref. [88].

GW150914 allows us to search for evidence of dispersion as the signal propagated toward the Earth. We perform the analysis by explicitly including the formally 1PN-order term above [88, 92] in the EOBNR and IMRPhenom GW phases and treating λ_g as an additional, independent parameter [93]. We assume a standard ΛCDM cosmology [94] and a uniform prior probability on the graviton mass $m_g \in [10^{-26}, 10^{-16}]$ eV/c^2, thus the prior on λ_g is $\propto 1/\lambda_g^2$. In Fig. 8 we show the cumulative posterior probability distribution for λ_g obtained from combining the results of the two waveform models (EOBNR and IMRPhenom) following the procedure outlined in Ref. [3]. We find no evidence for a finite value of λ_g and we place a lower dynamical bound of 10^{13} km at 90% confidence, which corresponds to a graviton mass $m_g \leq 1.2 \times 10^{-22}$ eV/c^2 at 90% confidence. This bound is approximately a factor of three better than the current Solar-System bound [87, 88], and $\sim$ three orders of magnitude better than the one from binary-pulsar observations [91], but it is less constraining than model-dependent bounds coming from the large-scale dynamics of galactic clusters [89] and weak gravitational-lensing observations [90].

No constraint on non-GR polarization states. GR predicts the existence of two transverse traceless tensor polarizations for GWs. More general metric theories of gravitation allow for up to four additional polarization states: a transverse scalar mode and up to three longitudinal modes [13, 95]. Because of the similar orientations of the Hanford and Livingston LIGO instruments, our data cannot exclude the presence of non-GR polarization states in GW150914. As an illustration, we use the BayesWave GW-transient analysis algorithm [51] to reconstruct the GW150914 signal, assuming the simplest nonphysical case in which the signal model consists of purely a scalar mode. We compare the reconstructed waveforms for the pure scalar-mode and GR models, and find the Bayes factor between the two hypotheses to be statistically consistent, the only notable difference being the reconstructed sky locations. The latter reflects the different response of the detector network to the transverse components of the polarization tensor compared the pure scalar mode. This agrees with the comprehensive parameter-estimation studies of GW150914 [3], which include only the transverse traceless GR polarizations. In effect, the LIGO Hanford–Livingston network records a single linear combination of the GR polarizations; as a consequence, both face-on and face-off binary inclinations are consistent with the data—see Fig. 2 in Ref. [3]. In the absence of an electromagnetic or neutrino counterpart, we conclude that determining the polarization content of signals like GW150914 will require a network including detectors with different orientations, such as Virgo [96].

Outlook. The observation of GW150914 has given us the opportunity to perform quantitative tests of the genuinely strong-field dynamics of GR. We investigated the nature of GW150914 by performing a series of tests devised to detect inconsistencies in the predictions of GR. With the exception of the graviton Compton wavelength and the test for the presence of a non-GR polarization, we did not perform any study aimed at constraining parameters that might arise from specific alternative theories to GR [13, 14, 85], such as Einstein-æther theory [97] and dynamical Chern–Simons [98], or from compact-object binaries composed of exotic objects such as boson stars [99] or gravastars [100]. Studies of this kind are not possible yet, since we lack predictions for what the inspiral-merger-ringdown GW signal should look like in those cases. We hope that the observation of GW150914 will boost the development of such models in the near future.

We will attempt to measure more than one damped sinusoid from the data after GW150914's peak, thus extracting the QNMs and inferring the final black-hole's mass and spin. We will, thus, be able to test the no-hair theorem [65, 66] and the second law of black-hole dynamics [70, 71]. However, signals louder than GW150914 might be needed to achieve these goals. GR predicts the existence of only two transverse polarizations for GWs. In the future, we plan to investigate whether an extended detector network will allow the measurement of non-transverse components [13] in further GW signals.

The constraints provided by GW150914 on deviations from GR are unprecedented due to the nature of the source, but they do not reach high precision for some types of deviation, particularly those affecting the inspiral regime. A much higher SNR and longer signals are necessary for more stringent tests. However, it is not clear up to which SNR our parameterized waveform models are still a faithful representation of solutions of Einstein's equations. Furthermore, to extract physical effects we need waveform models that are parameterized in terms of those physical effects. We hope that, following GW150914, further efforts will be made to develop reliable, physical and computationally fast waveform models. More stringent bounds can be obtained by combining results from multiple GW observations [58, 82, 83, 93]. Given the rate of coalescence of binary black holes as inferred in Ref. [101], we are looking forward to the upcoming joint observing runs of LIGO and Virgo.

The detection of GW150914 ushers in a new era in the field of experimental tests of GR: within the limits set by our sensitivity, all the tests we have performed provided no evidence against the predictions of GR.

Acknowledgments. The authors gratefully acknowledge the support of the United States National Science Foundation (NSF) for the construction and operation of the LIGO Laboratory and Advanced LIGO as well as the Science and Technology Facilities Council (STFC) of the United Kingdom, the Max-Planck-Society (MPS), and the State of Niedersachsen/Germany for support of the construction of Advanced LIGO and construction and operation of the GEO600 detector. Additional support for Advanced LIGO was provided by the Australian Research Council. The authors gratefully acknowledge the Italian Istituto Nazionale di Fisica Nucleare (INFN), the French Centre National de la Recherche Scientifique (CNRS) and the Foundation for Fundamental Research on Matter supported by the Netherlands Organisation for Scientific Research, for the construction and operation of the Virgo detector and the creation and support of the EGO consortium. The authors also gratefully acknowledge research support from these agencies as well as by the Council of Scientific and Industrial Research of India, Department of Science and Technology, India, Science & Engineering Research Board (SERB), India, Ministry of Human Resource Development, India, the Spanish Ministerio de Economía y Competitividad, the Conselleria d'Economia i Competitivitat and Conselleria d'Educació, Cultura i Universitats of the Govern de les Illes Balears, the National Science Centre of Poland, the European Commission, the Royal Society, the Scottish Funding Council, the Scottish Universities Physics Alliance, the Hungarian Scientific Research Fund (OTKA), the Lyon Institute of Origins (LIO), the National Research Foundation of Korea, Industry Canada and the Province of Ontario through the Ministry of Economic Development and Innovation, the Natural Science and Engineering Research Council Canada, Canadian Institute for Advanced Research, the Brazilian Ministry of Science, Technology, and Innovation, Russian Foundation for Basic Research, the Leverhulme Trust, the Research Corporation, Ministry of Science and Technology (MOST), Taiwan and the Kavli Foundation. The authors gratefully acknowledge the support of the NSF, STFC, MPS, INFN, CNRS and the State of Niedersachsen/Germany for provision of computational resources.

[1] B. Abbott et al., Phys. Rev. Lett. **116**, 061102 (2016), https://dcc.ligo.org/LIGO-P150914/public/main.
[2] B. Abbott et al. (2016), https://dcc.ligo.org/LIGO-P1500269/public/main.
[3] B. Abbott et al. (2016), https://dcc.ligo.org/LIGO-P1500218/public/main.
[4] J. Kepler, *Astronomia nova ..., seu physica coelestis, tradita commentariis de motibus stellae martis* (1609).
[5] I. Newton, *Philosophiae Naturalis Principia Mathematica* (1687).
[6] A. Einstein, Preuss. Akad. Wiss. Berlin p. 688 (1916).
[7] A. Einstein, Preuss. Akad. Wiss. Berlin p. 154 (1918).
[8] R. A. Hulse and J. H. Taylor, Astrophys. J. Lett. **195**, L51 (1975).
[9] J. H. Taylor and J. M. Weisberg, Astrophys. J. **253**, 908 (1982).
[10] L. Blanchet, Living Rev. Rel. **17**, 2 (2014).
[11] M. Burgay et al., Nature **426**, 531 (2003).
[12] N. Wex (2014), arXiv:1402.5594.
[13] C. M. Will, Living Rev. Rel. **17**, 4 (2014).
[14] E. Berti et al., Class. Quant. Grav. **32**, 243001 (2015).
[15] T. Damour and G. Esposito-Farese, Class. Quant. Grav. **9**, 2093 (1992).
[16] P. C. C. Freire et al., Mon. Not. Roy. Astron. Soc. **423**, 3328 (2012).
[17] K. Schwarzschild, Sitzungsber. Preuss. Akad. Wiss. Berlin (Math. Phys.) **1916**, 189 (1916).
[18] R. P. Kerr, Phys. Rev. Lett. **11**, 237 (1963).
[19] A. Buonanno and T. Damour, Phys. Rev. D **59**, 084006 (1999).
[20] A. Buonanno and T. Damour, Phys. Rev. D **62**, 064015 (2000).
[21] T. Damour, P. Jaranowski, and G. Schaefer, Phys. Rev. **D78**, 024009 (2008).
[22] T. Damour and A. Nagar, Phys. Rev. **D79**, 081503 (2009).
[23] E. Barausse and A. Buonanno, Phys. Rev. **D81**, 084024 (2010).
[24] F. Pretorius, Phys. Rev. Lett **95**, 121101 (2005).
[25] M. Campanelli, C. O. Lousto, P. Marronetti, and Y. Zlochower, Phys. Rev. Lett **96**, 111101 (2006).
[26] J. G. Baker, J. Centrella, D.-I. Choi, M. Koppitz, and J. van Meter, Phys. Rev. Lett **96**, 111102 (2006).
[27] C. V. Vishveshwara, Nature **227**, 936 (1970).
[28] W. H. Press, Astrophys. J. **170**, L105 (1971).
[29] S. Chandrasekhar and S. L. Detweiler, Proc. Roy. Soc. Lond. **A344**, 441 (1975).
[30] Y. Pan, A. Buonanno, J. G. Baker, J. Centrella, B. J. Kelly, S. T. McWilliams, F. Pretorius, and J. R. van Meter, Phys. Rev. **D77**, 024014 (2008).
[31] P. Ajith et al., Phys. Rev. **D77**, 104017 (2008), [Erratum: Phys. Rev.D79,129901(2009)].
[32] P. Ajith et al., Phys. Rev. Lett. **106**, 241101 (2011).
[33] L. Santamaria et al., Phys. Rev. **D82**, 064016 (2010).
[34] A. Taracchini et al., Phys. Rev. **D89**, 061502 (2014).
[35] A. H. Mroué et al., Phys. Rev. Lett. **111**, 241104 (2013).
[36] M. Pürrer, Class. Quant. Grav. **31**, 195010 (2014).
[37] M. Pürrer (2015), arXiv:1512.02248.
[38] S. Husa, S. Khan, M. Hannam, M. Pürrer, F. Ohme, X. J. Forteza, and A. Bohé (2015), arXiv:1508.07250.
[39] S. Khan, S. Husa, M. Hannam, F. Ohme, M. Pürrer, X. J. Forteza, and A. Bohé (2015), arXiv:1508.07253.
[40] M. Hannam, P. Schmidt, A. Bohé, L. Haegel, S. Husa, F. Ohme, G. Pratten, and M. Pürrer, Phys. Rev. Lett. **113**, 151101 (2014).
[41] P. Kumar, T. Chu, H. Fong, H. P. Pfeiffer, M. Boyle, D. A. Hemberger, L. E. Kidder, M. A. Scheel, and B. Szilagyi (2016), arXiv:1601.05396.
[42] B. Abbott et al. (2016), https://dcc.ligo.org/P1500259/public/main.
[43] B. Bruegmann, J. A. Gonzalez, M. Hannam, S. Husa, U. Sperhake, and W. Tichy, Phys. Rev. **D77**, 024027 (2008).
[44] R. O'Shaughnessy, L. London, J. Healy, and D. Shoemaker, Phys. Rev. **D87**, 044038 (2013).
[45] M. A. Scheel, M. Giesler, D. A. Hemberger, G. Lovelace, K. Kuper, M. Boyle, B. Szilgyi, and L. E. Kidder, Class. Quant. Grav. **32**, 105009 (2015).
[46] T. Chu, H. Fong, P. Kumar, H. P. Pfeiffer, M. Boyle, D. A. Hemberger, L. E. Kidder, M. A. Scheel, and B. Szilagyi (2015), arXiv:1512.06800.
[47] C. O. Lousto, J. Healy, and H. Nakano (2015), arXiv:1508.04768.
[48] B. Szilgyi, J. Blackman, A. Buonanno, A. Taracchini, H. P. Pfeiffer, M. A. Scheel, T. Chu, L. E. Kidder, and Y. Pan, Phys. Rev. Lett. **115**, 031102 (2015).
[49] B. Abbott et al. (2016), https://dcc.ligo.org/LIGO-P1500229/public/main.
[50] J. Veitch et al., Phys.Rev. **D91**, 042003 (2015).
[51] N. J. Cornish and T. B. Littenberg, Class. Quant. Grav. **32**, 135012 (2015).
[52] M. Vallisneri and N. Yunes, Phys. Rev. D **87**, 102002 (2013).
[53] S. Vitale and W. Del Pozzo, Phys. Rev. D **89**, 022002 (2014).

[54] T. A. Apostolatos, Phys. Rev. D **52**, 605 (1995).
[55] N. Cornish, L. Sampson, N. Yunes, and F. Pretorius, Phys. Rev. D **84**, 062003 (2011).
[56] M. Vallisneri, Phys. Rev. D **86**, 082001 (2012).
[57] J. Healy, C. O. Lousto, and Y. Zlochower, Phys. Rev. D **90**, 104004 (2014).
[58] A. Ghosh, A. Ghosh, N. K. Johnson-McDaniel, C. K. Mishra, P. Ajith, W. Del Pozzo, D. A. Nichols, Y. Chen, A. B. Nielsen, C. P. L. Berry, et al. (2016), 1602.02453.
[59] B. Allen, Phys. Rev. **D71**, 062001 (2005).
[60] Y. Pan, A. Buonanno, M. Boyle, L. T. Buchman, L. E. Kidder, H. P. Pfeiffer, and M. A. Scheel, Phys. Rev. **D84**, 124052 (2011).
[61] E. Berti, V. Cardoso, and C. M. Will, Phys. Rev. **D73**, 064030 (2006).
[62] A. Buonanno, G. B. Cook, and F. Pretorius, Phys. Rev. D **75**, 124018 (2007).
[63] E. Berti, V. Cardoso, J. A. Gonzalez, U. Sperhake, M. Hannam, S. Husa, and B. Bruegmann, Phys. Rev. **D76**, 064034 (2007).
[64] I. Kamaretsos, M. Hannam, S. Husa and B. S. Sathyaprakash, Phys. Rev. D **85**, 024018 (2011).
[65] W. Israel, Phys. Rev. **164**, 1776 (1967).
[66] B. Carter, Phys. Rev. Lett. **26**, 331 (1971).
[67] O. Dreyer, B. J. Kelly, B. Krishnan, L. S. Finn, D. Garrison, and R. Lopez-Aleman, Class. Quant. Grav. **21**, 787 (2004).
[68] S. Gossan, J. Veitch, and B. Sathyaprakash, Phys. Rev. D **85**, 124056 (2012).
[69] J. Meidam, M. Agathos, C. Van Den Broeck, J. Veitch, and B. S. Sathyaprakash, Phys. Rev. **D90**, 064009 (2014).
[70] S. W. Hawking, Phys. Rev. Lett. **26**, 1344 (1971).
[71] J. M. Bardeen, B. Carter, and S. W. Hawking, Commun. Math. Phys. **31**, 161 (1973).
[72] L. Blanchet and G. Schaefer, Class. Quant. Grav. **10**, 2699 (1993).
[73] L. Blanchet, Class. Quant. Grav. **15**, 113 (1998), [Erratum: Class. Quant. Grav.22,3381(2005)].
[74] J. Lense and H. Thirring, Physikalische Zeitschrift **19**, 156 (1918).
[75] B. M. Barker and R. F. O'Connell, Phys. Rev. D **12**, 329 (1975).
[76] L. E. Kidder, Phys. Rev. **D52**, 821 (1995).
[77] L. Blanchet and B. S. Sathyaprakash, Classical and Quantum Gravity **11**, 2807 (1994).
[78] L. Blanchet, T. Damour, and B. R. Iyer, Phys. Rev. D **51**, 5360 (1995).
[79] K. G. Arun, B. R. Iyer, M. S. S. Qusailah, and B. S. Sathyaprakash, Phys. Rev. **D74**, 024006 (2006).
[80] C. K. Mishra, K. Arun, B. R. Iyer, and B. Sathyaprakash, Phys. Rev. D **82**, 064010 (2010).
[81] N. Yunes and F. Pretorius, Phys. Rev. D **80**, 122003 (2009).
[82] T. Li, W. Del Pozzo, S. Vitale, C. Van Den Broeck, M. Agathos, et al., Phys.Rev. **D85**, 082003 (2012).
[83] M. Agathos, W. Del Pozzo, T. G. F. Li, C. Van Den Broeck, J. Veitch, and S. Vitale, Phys. Rev. D **89**, 082001 (2014).
[84] N. Yunes and S. A. Hughes, Phys. Rev. D **82**, 082002 (2010).
[85] N. Yunes and X. Siemens, Living Rev. Rel. **16**, 9 (2013).
[86] C. de Rham, Living Rev. Rel. **17**, 7 (2014).
[87] C. Talmadge, J. P. Berthias, R. W. Hellings, and E. M. Standish, Phys. Rev. Lett. **61**, 1159 (1988).
[88] C. M. Will, Phys. Rev. D **57**, 2061 (1998).
[89] A. S. Goldhaber and M. M. Nieto, Phys. Rev. D **9**, 1119 (1974).
[90] S. R. Choudhury, G. C. Joshi, S. Mahajan, and B. H. J. McKellar, Astropart. Phys. **21**, 559 (2004).
[91] L. S. Finn and P. J. Sutton, Phys. Rev. **D65**, 044022 (2002).
[92] D. Keppel and P. Ajith, Phys. Rev. D **82**, 122001 (2010).
[93] W. Del Pozzo, J. Veitch, and A. Vecchio, Phys. Rev. D **83**, 082002 (2011).
[94] P. A. R. Ade et al. (Planck) (2015), arXiv:1502.01589.
[95] D. M. Eardley, D. L. Lee, A. P. Lightman, R. V. Wagoner, and C. M. Will, Phys. Rev. Lett. **30**, 884 (1973).
[96] F. Acernese et al. (Virgo), Class. Quant. Grav. **32**, 024001 (2015).
[97] T. Jacobson and D. Mattingly, Phys. Rev. **D64**, 024028 (2001).
[98] S. Alexander and N. Yunes, Phys. Rept. **480**, 1 (2009).
[99] S. L. Liebling and C. Palenzuela, Living Rev. Rel. **15**, 6 (2012).
[100] P. O. Mazur and E. Mottola, Proc. Nat. Acad. Sci. **101**, 9545 (2004).
[101] B. Abbott et al. (2016), https://dcc.ligo.org/LIGO-P1500217/public/main.